DEPARTMENT OF OCEAN ENGINEERING

MASSACHUSETTS INSTITUTE OF TECHNOLOGY

CAMBRIDGE, MASSACHUSETTS 02139

MATERIAL DEGRADATION IN HEAVY STEEL PLATES
CAUSED BY BENDING WITH A LASER

by

DEBRA LEE DEACON
Lieutenant, U. S. Navy

SM(NA&ME)
OE

Course 13A
June, 1984

Copy 3

Thesis
D18247

MATERIAL DEGRADATION IN HEAVY STEEL PLATES CAUSED BY BENDING WITH A LASER

by

DEBRA LEE DEACON

B.S. Chemistry, University of Wisconsin-Milwaukee
(1976)

SUBMITTED TO THE DEPARTMENT OF
OCEAN ENGINEERING
IN PARTIAL FULFILLMENT OF THE REQUIREMENTS
FOR THE DEGREES OF

OCEAN ENGINEER

and

MASTER OF SCIENCE IN
NAVAL ARCHITECTURE AND MARINE ENGINEERING

at the

MASSACHUSETTS INSTITUTE OF TECHNOLOGY
June, 1984

© Massachusetts Institute of Technology, 1984

The author hereby grants to agencies of the United States government permission to reproduce and to distribute copies of this thesis document in whole or in part.

Thesis
D18747

MATERIAL DEGRADATION IN HEAVY STEEL PLATES CAUSED BY BENDING WITH A LASER

by

DEBRA LEE DEACON

Submitted to the Department of Ocean Engineering
on May 11, 1984 in partial fulfillment of the
requirements for the Degrees of Ocean Engineer
and Master of Science in
Naval Architecture and Marine Engineering

ABSTRACT

A new process for bending heavy steel plates, using a laser to supply line heat, is described. A set of samples bent by this method was examined for metallurgical damage.

Metallographic examination revealed problems of grain grouwth and carbide segregation. Hardness measurements led to the conclusion that the heat affected zone is being transformed into untempered martensite. Microprobe analysis indicated a loss of nickel to carbide segregation. Charpy V-notch tests indicated a loss of ductility in the heat affected zone.

The extent of damage was found to be a function of the surface temperature produced by the laser. A multiple-pass procedure was found to do much less damage than a single-pass procedure for an equivalent degree of bend.

It is concluded that the process is feasible. Recommendations are made for further research.

Thesis Supervisor: Dr. Koichi Masubuchi

Title: Professor of Ocean Engineering

TABLE OF CONTENTS

1. Introduction

2. The Process

3. The Metallurgy of HY-80 Steel Plates

4. Metallography of the Bent Plates

5. Microhardness Examination of the Bent Plates

6. Notch Toughness of the Bent Plates

7. Chemical Analysis of the Bent Plates

8. Conclusions

LIST OF FIGURES

1. Simplified Model of Absorbance versus Power Density
2. Time/Power Regimes for Current Processes
3. Experimental Arrangement
4. Drawing of Workpiece
5. Heat Input versus Degree of Bend
6. Iron-Carbon Phase Diagram
7. Continuous Cooling Diagram
8. Schematic of Quench-and-Tempering Process
9. Graph of the Physical Properties of Tempered Martensite
10. Diagram of Metallographic Samples
11. Photograph of Plate 2, Irradiated Edge, 40x
12. Photograph of Plate 2, Bottom of Heat Affected Zone, 40x
13. Photograph of Plate 2, Unaffected Baseplate, 40x
14. Photograph of Plate 2, Irradiated Edge, 1000x
15. Photograph of Plate 2, Zone 1, 1000x
16. Photograph of Plate 2, Mixed Region, 1000x
17. Photograph of Plate 2, Unaffected Baseplate, 1000x
18. Photograph of Plate 3, Irradiated Edge, 1000x
19. Photograph of Plate 1, Irradiated Edge, 1000x

LIST OF FIGURES (CONTINUED)

20. Photograph of Plate 1, Mixed Region, 1000x

21. Half-Angle of Bend versus Depth of Visible Damage

22. Heat Input versus Depth of Visible Damage

23. Microhardness versus Depth for Single-Pass Bends

24. Microhardness versus Depth for Multiple-Pass Bends

25. Surface Hardness Across Burn on Plate 2

26. Diagram of Charpy Bars

27. Charpy V-Notch versus Temperature for Control Sample

28. Charpy V-Notch versus Temperature for Center of Beam Path

29. Charpy V-Notch versus Temperature for Edge of Beam Path

30. Chemical Line Analysis of Plate 1

31. Chemical Line Analysis of Plate 2

32. Recommended Laser Power - Travel Speed Combinations

LIST OF TABLES

1. Laser Parameters and Degree of Bend
2. Initial Estimates of Temperature and Heat Input
3. Chemical Composition of HY-80
4. Ductile Requirements for HY-80
5. Depth of Visible Damage
6. Microhardness of Plate 1
7. Microhardness of Plate 2
8. Microhardness of Plate 3
9. Microhardness of Plate 4
10. Microhardness of Plate 5
11. Surface Hardness of Plate 2
12. Summary of Charpy Tests
13. Chemical Line Analysis of Plate 1
14. Chemical Line Analysis of Plate 2

1. INTRODUCTION

The fabrication of a ship hull, particularly a submarine hull, requires that gradual and complex curves be made in very heavy plates of steel. Currently, plate bending is normally accomplished with a very large brake press. This results in a highly cold-worked plate that only roughly approximates the desired final shape. Traditionally, complex curves were made in mild steels by line-heating with an oxy-acetylene torch. In the hands of a skilled shipfitter, very good shapes were obtained. Unfortunately, this is a dying art in modern shipyards. The majority of hulls for naval vessels are made of a quench-and-tempered steel called HY-80. To preserve the special properties of this alloy, extreme controls are placed upon any process involving heat input. Line bending by oxy-acetylene torch is forbidden on these materials, and therefore rarely practiced.

Line heating is also the most convenient way to straighten metal assemblies that have been distorted by welding.

The mechanism is the same whether one is line heating to induce a deliberate bend or to remove an undesired bend.

It was suggested by Professor Masubuchi[1] that the

inherent controllability of the laser combined with its high power density would permit predictable plate bending with minimal material damage. A project was established to explore the potential of a laser process to bend heavy steel plates. This document presents the background research on HY-80 steel and the probable effects of bending with laser. Additionally, the results of metallurgical examination of an initial series of experimental plate bends are included.

2. THE PROCESS

The laser has many advantages over the oxyacetylene torch as a source of heat. The power is very concentrated, limiting the volume of heating to the very surface of the plate. Therefore, any material degradation can be expected to be limited to the surface of the plate. The heat input can be exactly controlled and is much more reproducible than torch heating. Also, laser systems lend themselves more readily to automation.

There are, of course, certain disadvantages associated with the use of lasers. The high powers necessary for metal working demand a very large laser. A state-of-the-art high power laser currently fills a good-sized room. The high power inputs also require more careful control in view of the greater capacity for damage. The high energy beam of a CO_2 laser, the type used for metal working, cannot be directed with fiber optics. Mirrors must be used to direct the energy onto the workpiece. Current installations are all remotely operated. There is yet no safe way to direct the beam with a hand tool. Finally, the initial investment in a high energy laser and its accessories for metal working is much higher than the investment required for torch bending. However, it should not be much higher than the massive brake-presses currently required for bending quench-

and-tempered steel plates.

When a metal surface in irradiated by a laser beam, some of the incident energy is absorbed into the surface and the remainder is reflected (neglecting very small scale shockwave effects). The absorbed energy penetrates from a surface layer on the order of .0001 mm thick into the mass by thermal conduction[2].

The fraction of the energy absorbed depends upon the surface finish and the frequency of the laser beam. Absorbance is quite low for clean, shiny metal surfaces[3]. At the frequency of the CO_2 laser, 10.6 microns, most metals are not very absorbant at room temperature. As the temperature increases, the absorbance gradually increases to 40-50% at the melting point. Then the absorbance rapidly increases to nearly 100%. Absorbant coatings are often used to increase the absorbance to as much as 95%.

Figure 1 is a simplified model of absorbance versus power density for metal processing at 10.6 microns[4].

The heating effects of laser depend on the thermal properties of the irradiated surface and the beam parameters of the laser. The spectrum of effects can be divided roughly into three regions.

At low power densities, the material is heated, but does not reach the melting point. The effects of processes in this region are entirely controlled by the material

properties. The laser can be treated like any other heat source. Processes in this range include surface hardening and the bending process currently being investigated.

At moderate power densities, the surface melts and a fluid front propagates into the mass. The depth of the melted region is a function of the power density up to the point where surface vaporization begins. The depth that can be melted without vaporization is quite shallow. It is generally desired to limit vaporization of the metal during welding; so the maximum power that can be used without vaporization places an upper limit on the power that can be used for welding. Moderate power densities are used for welding, cladding and surface glazing.

The high power region is that above the vaporization threshold. Vaporization is desired for drilling holes and machining with a laser. With a continuous wave laser, vaporization occurs at the material's normal boiling point and the vapor has time to diffuse away from the work site. If vaporization is performed with a higher power pulse laser, a plume of vaporized material develops. This plume decreases the amount of laser radiation reaching the surface on subsequent pulses. As a result, the depth of drilling is much reduced from holes drilled with lower power. The highest energy irradiation causes the emission of a charged particle plasma. High power is used for drilling,

machining, surface glazing and shock hardening[5].

Figure 2 shows the time/power regimes for current processes including the line-bending experiments[6]. The process of line heat plate bending is the same regardless of the heat source.

Upon applying heat to one surface, thermal expansion takes place throughout the plate. But the heated surface, for convenience let us say the top of the plate, expands more the the opposite surface. The top surface experiences compressive stresses and local plastic yielding occurs to relieve it. Upon cooling, the thermal expansion is gradually eliminated, but the plastic deformation remains. The plate deflection goes through the zero point and ends with a concave bend and equilibrium of the stresses through the thickness.

The deformation process is the same for welding, flame cutting or bending.

For this investigation, a series of HY-80 plates were bent with a 15 kW continuous-wave CO_2 laser at the Naval Research Laboratory in Washington, D.C. The frequency of the beam was 10.6 microns. The laser beam was generated in one room and directed to the workpiece in the next room with a system of mirrors. At each mirror, there is a loss of power from the beam. The entire system has a 10% loss to the optics. A secondary laser with a beam within the

visible spectrum and a common optical path was used for focusing and beam alignment.

The workpiece was a sandblasted plate of HY-80, 12 inches long, 6 inches wide and 1/2 inch thick. The plate was painted to improve the absorbance. It was cantilevered from a clamped short end. The beam path was normal to the plane of the plate. The workpiece was attached to a motorized table.

The laser was started over the plate. During the run, the laser beam was stationary while the workpiece moved. Line heat was applied along the short axis of the plate, approximately halfway down the long side. Heat input was controlled by both the beam power level and the rate of workpiece travel.

Figure 3 shows the experimental arrangement. Figure 4 is a drawing of the workpiece.

A total of 7 pieces of plate were bent for this investigation. Five of the pieces had a single bend in the center of the plate. Both single pass and multiple pass bends were produced. Full metallographic examination was made of this set of plates. Two other plates were bent in the initial trials. These plates each had 2 bends about 6 inches apart along the short axis. There was no beam data recorded for these plates, but metallographic examination was used to determine the depth of any damaged area and one

of the plates was cut up for Charpy notch-toughness testing.

Table 1 is a listing of the experimental parameters and the degree of bend produced for the set of 5 plates.

Initial estimates were made of the surface temperature produced at the center of the beam path using a formula developed by John F. Ready[7].

$$T(0,0,t) = (Fd/K\pi^{1/2}) * \arctan (4kt/d^2)^{1/2}$$

K = thermal conductivity $\cong$ 10.016 J/s ft °C
k = thermal diffusivity $\cong$ .000126 ft^2/s
d = beam radius $\cong$ .0667 ft
t = irradiation duration = 2 * d / travel speed
F = beam flux density
= 7 kW * 1000 J/s kW * .9 (loss to optics) / .0139 ft^2
$\cong$ 453600 J/s ft^2

The heat input was estimated by the formula:

$$H = F * a * \pi * d^2 * t$$

H = heat input
a = absorbance of metal $\cong$ .30

The actual absorbance of this metal under the conditions of the experiment has not been determined. The plates were painted to improve the coupling, so it is greater than 10%. The value of 30% was chosen arbitrarily for this initial estimate. It may yield an over-estimate of the actual heat input.

The initial estimates for the series are presented in Table 2.

Figure 5 is a graph of the heat input versus the degree

of bend for both single pass bends and multiple pass bends. It is clear that a greater degree of bend is induced by a single pass method than a multiple pass method for the same total heat input. These results agree with data obtained by a Japanese study done of plate distortion by laser line heating performed in conjunction with an investigation of laser welding[8].

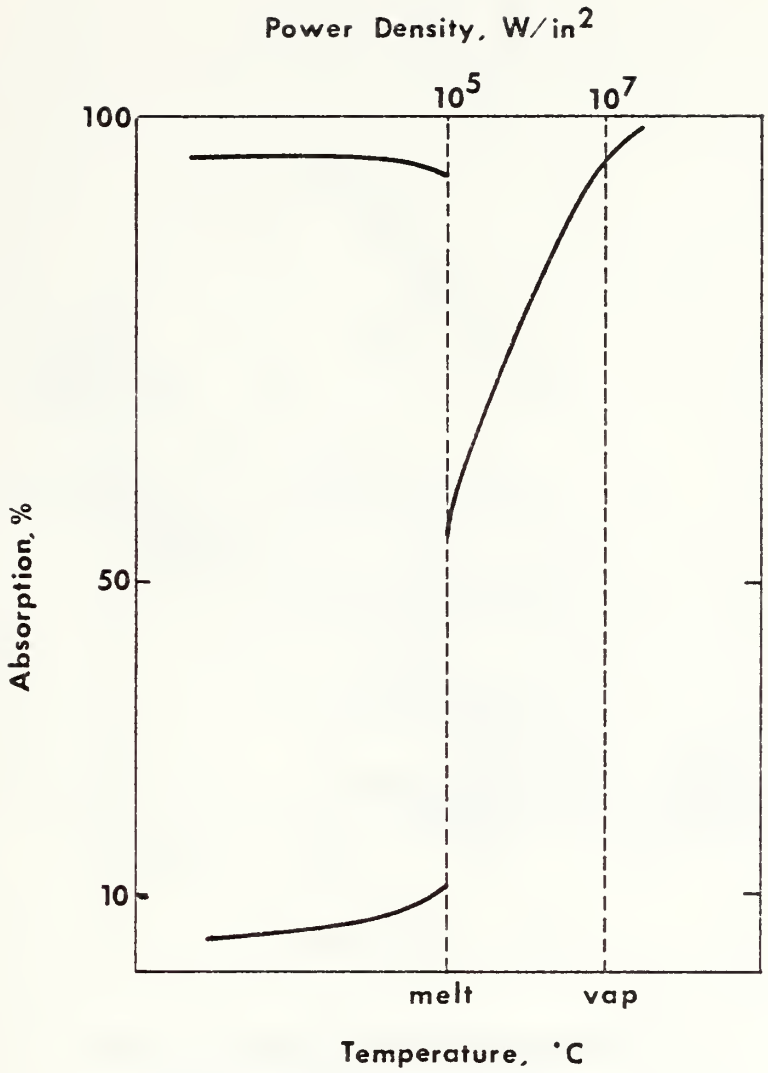

Simplified Model of Absorbance versus
Power Density for
CO_2 Laser Processes

FIGURE 1

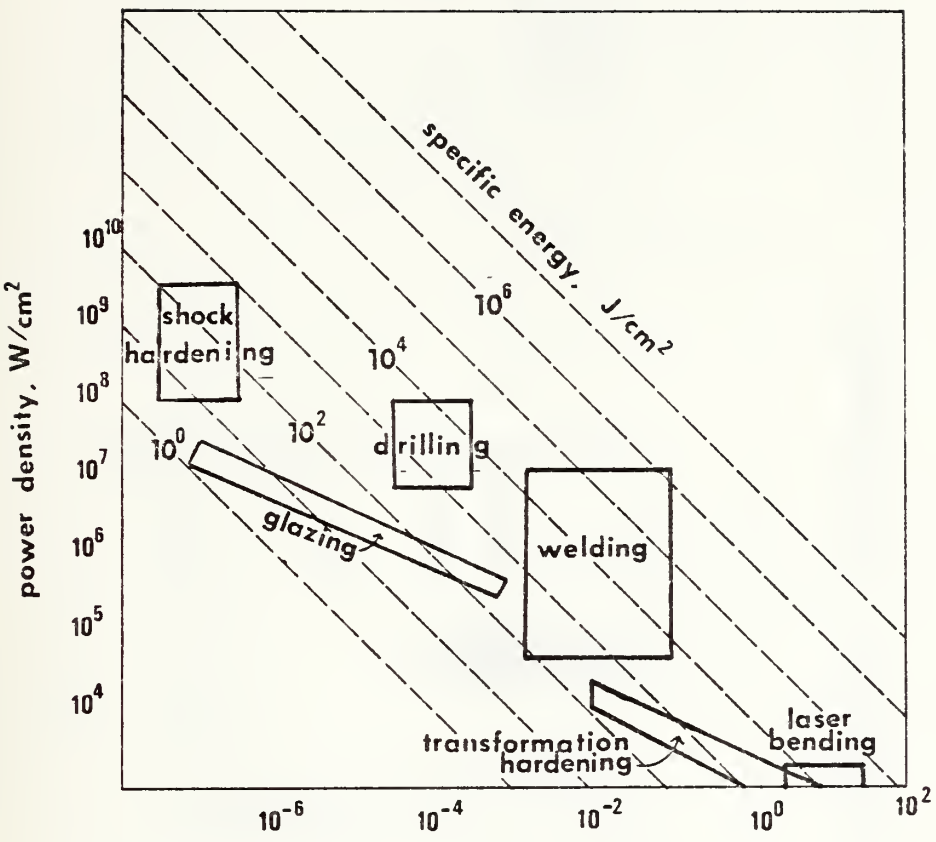

TIME / POWER DENSITY REGIMES FOR CURRENT LASER PROCESSES

FIGURE 2

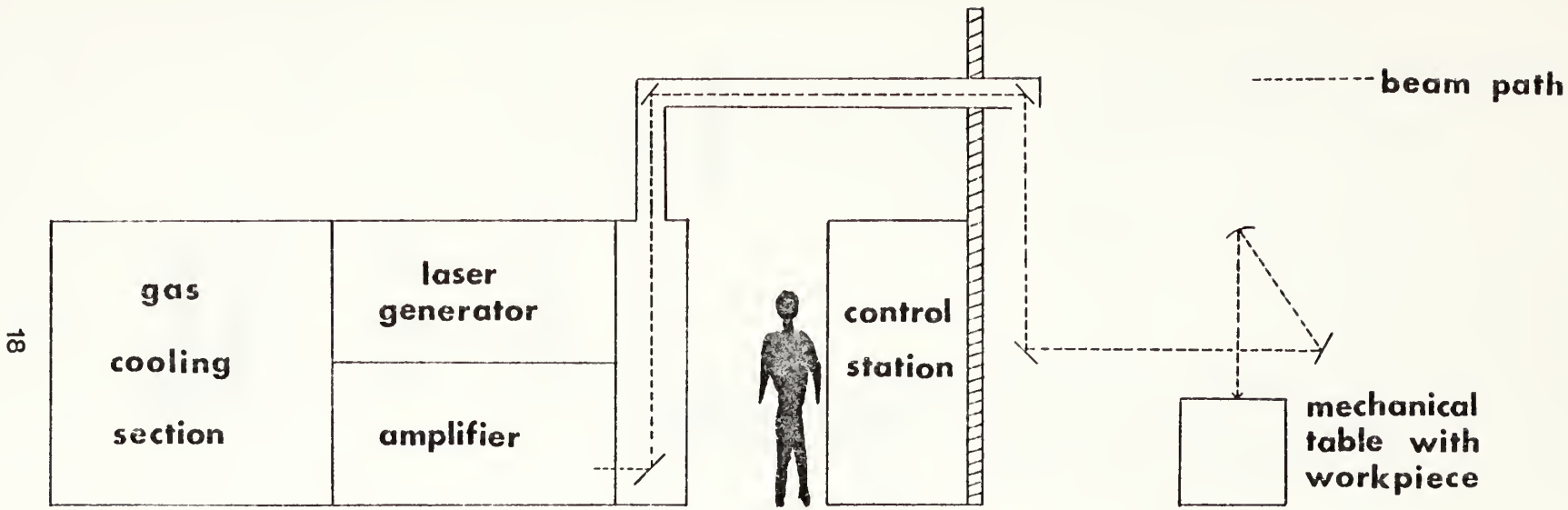

SKETCH OF EXPERIMENTAL ARRANGEMENT

FIGURE 3

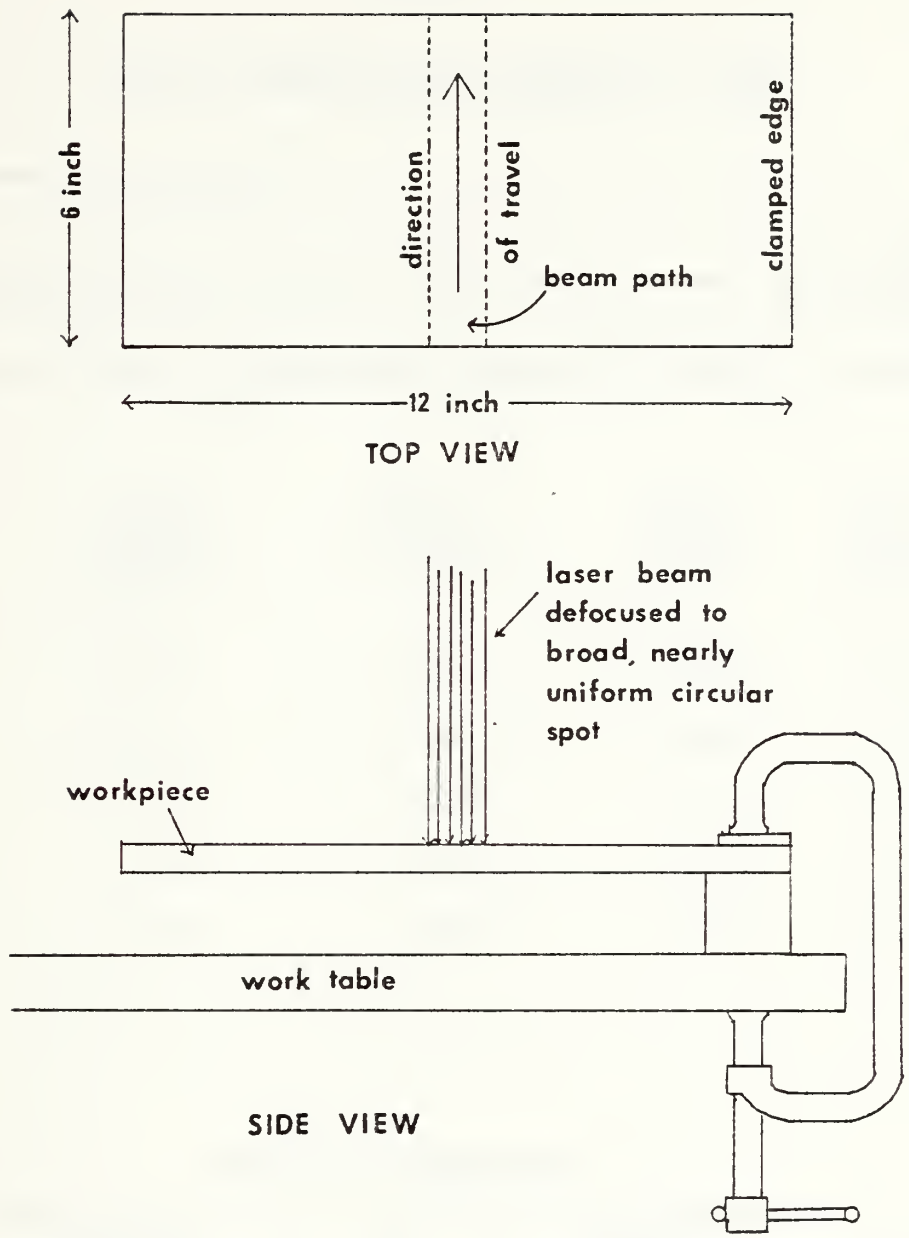

FIGURE 4
WORKPIECE

TABLE 1

LASER PARAMETERS AND DEGREE OF BEND

Common laser parameters:

Power.....7 kW
Beam shape....."top hat", close to uniform
Distance from focal mirror.....30 inches

All plates had no measureable deflection before bending

Plate Number	Travel Speed [in/min]	Central Deflection [in]	Plate Length [in]	Half Angle [degree]
1	12	0.031	11.56	0.31
2	6	0.078	12.00	0.75
3	9	0.047	11.56	0.46
4	12	0.047	12.00	0.45
5	12	0.063	11.56	0.62

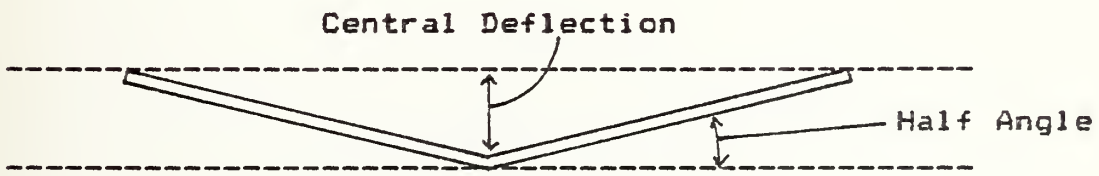

TABLE 2

INITIAL ESTIMATES OF TEMPERATURE AND HEAT INPUT

Plate Number	Travel Speed [ft/s]	Irradiation Duration [s]	Peak Temperature [°C]	Heat Input [J]
1	0.0167	7.988	1305	15193
2	0.0083	16.072	1609	30569
3	0.0125	10.672	1438	20298
4	0.0167	15.976	1305	30386
5	0.0167	23.964	1305	45580

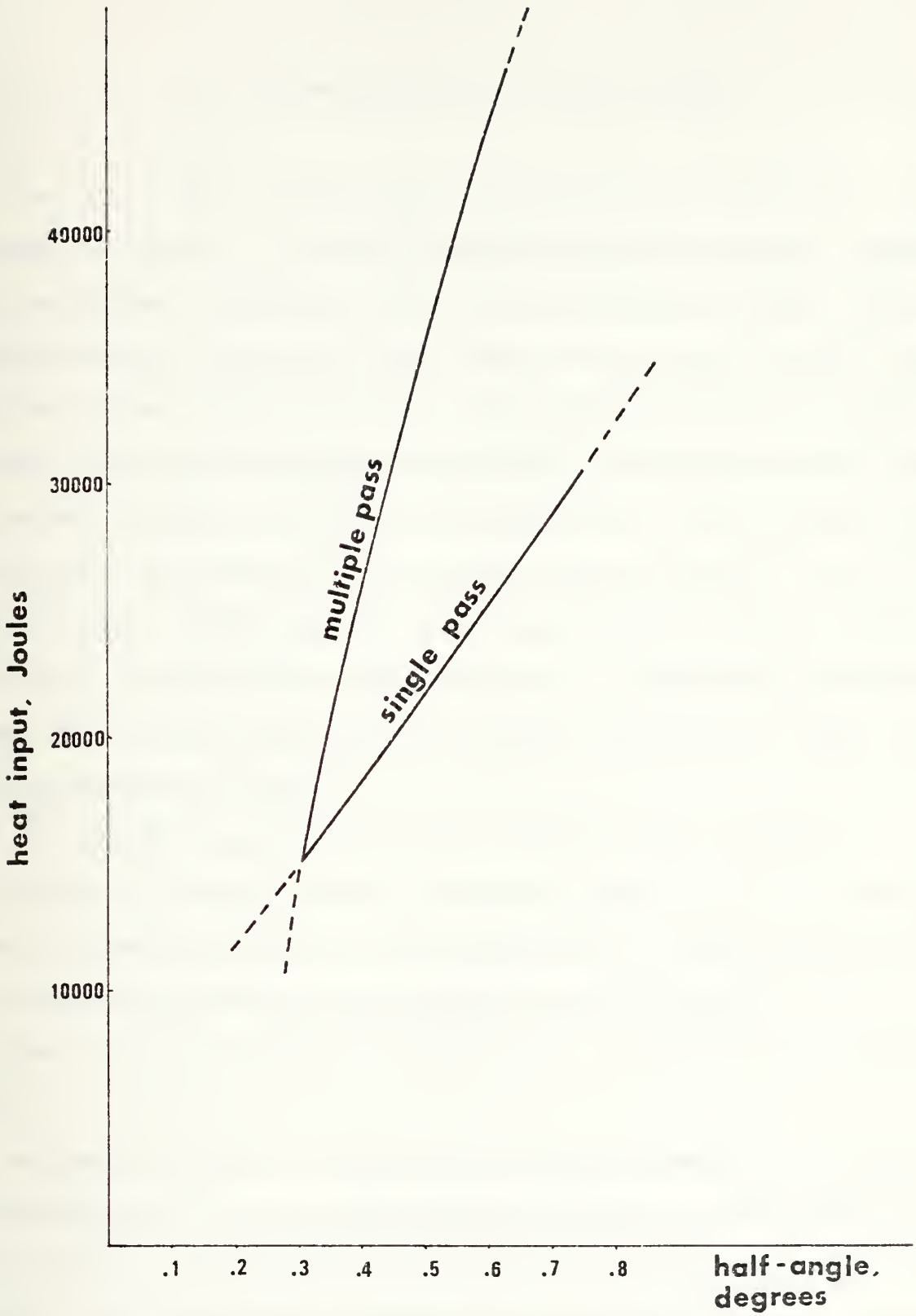

HEAT INPUT VS DEGREE OF BEND

FIGURE 5

3. THE METALLURGY OF HY-80 PLATES

In the early 1950's the need arose for a new steel for submarine hulls. The first specification for HY-80, based on low carbon STS armor plate, was drawn up in 1951. This specification called for cast ingots to be fully killed and grain-refined with aluminum. The plates rolled from these ingots were water-quenched from 900 °C, tempered at 650 °C and then water-quenched to ambient temperature. The plates were required to contain not less than 80% martensite at mid-thickness. HY-80 plates were required to have a yield strength of not less than 80,000 psi. Extruded structural tees meeting the specification became available in 1960, and rolled shapes in 1961[9].

The current specification for HY-80 is MIL-S-16216J.

HY-80 is a fully killed, low-alloy steel that is quench and tempered to obtain a microstructure of tempered bainite and tempered martensite throughout the thickness[10].

The required chemical composition is presented in Table 3[11].

Although carbon is not the alloying element in highest concentration, it has the greatest effect on the properties of a steel. It greatly increases the hardenability of the alloy, but it also increases the tendency to embrittlement of the heat affected zone of an arc weld. Therefore, its

concentration must be limited in a steel that will be used in large structures.

Nickel is the element that contributes most to the superior notch toughness of HY-80. It also makes a steel with a higher yield point, greater hardenability and higher impact and fatigue strengths.

Chrome is added primarily to improve wear and corrosion resistance. It also contributes to hardenability and yield strength. However, an alloy containing chrome has an increased tendency to temper embrittlement.

Molybdenum is added to the alloy to counter this tendency of the chrome. It also improves strength, hardenability and toughness.

The effects of the various alloying elements were learned by experience. The mechanism for the observed effect of the different elements is largely unknown. Nickel and chrome are known to produce complex carbides with iron that are less brittle and not quite as hard as iron carbide, which is a partial explanation to the hardenability and yield strength enhancement effects.

Nickel, chrome and molybdenum have the synergistic effect of pushing the bainite transformation line significantly to the right on a Continuous Cooling Transformation Diagram. This allows pure martensite to be produced with less stress-inducing quenching conditions. This is discussed in more

detail later in this chapter.

Silicon is present as a residual from the steelmaking process where it is used as a deoxidant. It has a neglible effect on the properties of the steel at such low concentrations.

Sulfur is an undesireable trace that is introduced as part of the ore and cannot be entirely removed from any steel. It forms a hard sulfide with iron that precipitates on the grain boundaries. This sulfide has a melting point low enough to be a problem in most common hot production processes. It is a major cause of cracking. To avoid formation of iron sulfide, manganese is added in a ratio of five parts manganese to one part sulfur, or greater.

Manganese also serves as a deoxidant. It increases the hardenability and the notch toughness of the alloy, and slightly enhances the corrosion resistance.

Phosphorus is another ubiquitous element that is introduced into the steel with the ore. It forms a phosphide with iron that is extremely brittle and segregates from the matrix, significantly reducing the strength of the alloy. There is no effective scavenger for phosphorus. As much as possible is burned off with oxygen in the steelmaking process, but the residual cannot be controlled as sulfur can be controlled with manganese. However, a very small amount of phosphorus, in the presence of copper,

enhances corrosion resistance[12,13] .

The specification for HY-80 limits the sum of the concentrations of phosphorus and sulfur to less than 0.035%.

Vanadium, titanium, copper, arsenic, tin and antimony may be present in very small amounts without adversely affecting the properties of the alloy[14].

The current specification requires vacuum degassing rather than aluminum ladle treatment. Liquid steel absorbs gases from the air. Upon cooling in the mold, these gases are rejected, leading to frothing and considerable inhomogeneity in the cast ingot. A "fully-killed" steel is one that has been degassed sufficiently so that there is no gas evolved in the mold. This results in a homogeneous structure in the finished product. Aluminum was used as a final degassing agent in earlier methods, but it was found to leave non-metallic inclusions in the ingot that can degrade the performance of the finished product[15].

The molten steel goes from the furnace to a ladle in which it is vacuum degassed. It is then poured into a mold and cooled to produce a large ingot. Plates are produced by hot rolling the ingot. These plates are then heat-treated to produce the desired properties in the plate[16].

The main constituents of any steel are iron, which is in the crystalline form of ferrite at room temperature, and

iron carbide, in the form of cementite. The properties of the steel depend primarily on the ratio of these two constituents and their distribution. Ferrite is iron with a small trace of carbon, along with any alloying elements, in solution. Cementite is iron carbide, a compound of iron and carbon that is very hard and brittle. Each grain in a steel contains both constituents.

Austenite is the high temperature crystalline form of these steels. It is a homogeneous solution of carbon in iron with no cementite present. This structure is not stable at room temperature[17].

Figure 6 is the iron-carbon phase diagram for the area of interest with HY-80. The alloying elements are all in low enough concentration to have no appreciable effect on the equilibrium lines. It can be seen that upon heating an alloy with a nominal carbon concentration of 0.18%, the transition temperature, where the alloy begins to turn to austenite, is at 727 °C. On continued heating, pure austenite is obtained by 842 °C. At 1490 °C, some of the austenite would break down into cementite in liquid iron solution, if the material were allowed to equilibrate. In the case of laser heating, equilibrium will not be attained. At 1495 °C, the austenite will begin to melt. By 1525 °C, the alloy would be fully liquid[18].

As the temperature increases above the transition

temperature, the grains of austenite grow larger. Final austenite grain size is a function of the temperature to which it is heated. The coarseness of the cooled steel is directly related to the austenite grain size prior to transformation.

Slow cooling from the austenite region results in the rejection of ferrite at the grain boundaries. The concentration of carbon in the grains increases until the alloy cools to the transition temperature. Below this, the grains assume a pearlite structure which is a lamellar arrangement of plates of ferrite and cementite.

With faster cooling, the alloy assumes a bainite structure in which the cementite grows in rods rather than plates in the ferrite matrix.

With still faster cooling, the alloy transforms into martensite. Martensite is a body - centered tetragonal crystal of iron carbide, while cementite is body-centered cubic. Martensite appears as rods or plates in the ferrite, not regular layers like cementite. The transformation involves no diffusion or composition change and is almost instantaneous. The percentage of martensite present depends only on the temperature to which the alloy is cooled. It is the hardest transformation product of austenite[19, 20].

Neither bainite nor martensite occur on the equilibrium phase diagram because they are metastable phases. Figure 7

is a graph of the transformation with continuous cooling for a similar alloy. It illustrates clearly the effect of cooling rate on the properties of the alloy[21]. Across the bottom of the diagram are the final constituents of the alloy for various cooling rates. To obtain pure martensite, the cooling rate must be faster the 8.3°C/sec. It should be emphasized that this is a particular case. For quenching from another temperature in the austenite region, a different cooling rate would be required. But the principle and general appearance of the diagram remain the same.

HY-80 plates are quench-and-tempered to obtain the desired properties of high yield strength, toughness and ductility. This is a heat treatment that involves heating to about 899°C., in the austenite region, followed by a water quench to ambient. This produces untempered martensite, which is very hard and very brittle. Martensite production involves an anisotropic expansion of the grains producing large residual stresses. To remove the residual stresses and restore some ductility and toughness, the plate is next tempered at 621-677°C. This also softens the metal somewhat. The temper is followed by a water quench[22].

Figure 8 is a schematic of the quench-and-tempering process.

Tempered martensite is formed when martensite is reheated to a temperature just below the transformation point. This

causes precipitation of spheroidal carbides dispersed in the ferrite matrix. The new structure has much improved ductility[23].

Figure 9 is a graph of the hardness, yield point, elongation and reduction of area of tempered martensite versus the ultimate yield strength[24].

Except for the requirement that a plate be at least 80% martensite at the midthickness, the specification makes no comment on the required microstructure, relying instead upon controlling the production process to obtain the desired characteristics in the plate.

A British team did a metallurgical examination of HY-80 in order to compare it with one of their submarine plates. They discovered two types of HY-80 plates. One type was composed of a mixture of tempered martensite and tempered bainite, the other was fully tempered martensite. Carbide precipitates were found in all the plates. Precipitates within the grains were found to be primarily iron carbide, while carbides of iron, nickel, chrome, manganese and molybdenum were found at the grain boundaries. Dark banding parallel to the rolling direction was found through the thickness of the plates. The Welding Institute, which also noted the characteristic banding, concluded that it was caused by segregation during ingot solidification. The segregated regions are flattened and spread out into bands

during the rolling process. The heat treatment then refines the grains without permitting much diffusion or solvation of the carbides. The result is a band of finely dispersed spherical carbide precipitates through the metal structure.

The individual grains of the alloy are also banded. These bands are alternating layers of martensite and bainite and intragranular carbide precipitates. Carbide precipitation is less in the bainite bands, giving them a lighter appearance under microscopic examination. Manganese sulfide inclusions have been found in the martensite bands and aluminum oxide inclusions have been found at the boundary between the light and dark bands.

Chemical analysis revealed that the plates that had the mixed martensite and bainite structure are lower in manganese, nickel, chrome and molybdenum than the plates that are completely martensite[25].

HY-80 owes its strength and toughness to its microstructure, which is the result of quench-and-tempering heat treatment.

The specification[26] for ductile properties are given in Table 4.

The requirements for notch toughness are quite extreme for a steel due to the critical nature of the structures in which it is used. Performing a Charpy V-notch test with a 10 x 10 mm bar, the force to break the sample must be

greater than:

35 ft-lb at -84.4 °C ± 1.7 °C

60 ft-lb at -17.8 °C ± 1.7 °C

The specification does not require a particular hardness for the finished plate, but it does supply the information that an acceptable plate will have a diamond pyramid hardness of 225-261[27].

The Welding Institute study found that the high nickel content and fully martensitic structure resulted in excellent fracture initiation behavior in comparison with other high strength steels. The fine grain structure and high angle grain boundaries act as barriers to propagation once a crack has started. In the mixed structure plates, the fracture tended to follow the tempered bainite bands. In the fully martensitic plates, the fractures followed the dark bands containing manganese sulfide inclusions[28].

HY-80 has been found to be susceptible to hydrogen induced cracking in the heat affected zone of a weld. Hydrogen cracking requires a sufficient concentration of hydrogen, the presence of tensile residual stresses, a susceptible microstructure and time to cool to ambient temperature[29].

Microcracking commonly occurs in the heat affected zone, adjacent to the fusion line, of weldments in HY-80. Masubuchi is quoted as believing it to be a result of grain

boundary liquation caused by inclusions. Savage believed that the cracks originated in a region of the weld metal. These are intergranular.

Delayed cracking can originate either in the heat affected zone or the weld metal. It characteristically occurs up to several days after welding. This transgranular form of cracking requires restraint and the presence of hydrogen[30].

The Welding Institute found that the primary factor in cracking in HY-80 is the inclusion population[31].

To maintain the desireable properties in HY-80 plate, certain restrictions are imposed upon subsequent manufacturing processes. Welding heat input is limited to 45000 J/inch for plates over 1/2 inch thick to ensure adequate notch toughness. Stress relieving temperatures are limited to the range of 593-621 °C followed by a rapid quench. Excessive time at temperatures between 371 °C and 482 C must be avoided to prevent temper embrittlement[32].

Although the conditions in the heat affected zone of a weld resemble the conditions in the heat affected zone of the laser bent plate, the closest analog is found in surface heat treatment for hardening, as reference to Figure 2 will show. Currently, induction, flame, laser and electron-beam are all used for surface heating. Regardless of the heat source, any surface heat treatment can affect fatigue

strength in two ways. It can cause chemical changes such that the material of the case has a higher fatigue strength than the core. It may cause compressive surface residual stresses that also increase fatigue strength. Therefore, the fatigue strength of the plate is likely to be improved by the laser bending process[33].

TABLE 3

CHEMICAL COMPOSITION OF HY-80

Element	to 1 1/4 inch thickness	from 1 1/4 inch thickness
Carbon	0.10-0.20	0.10-0.20
Manganese	0.10-0.45	0.10-0.45
Phosphorus	< 0.020	< 0.020
Sulfur	0.002-0.020	0.002-0.020
Silicon	0.12-0.38	0.12-0.38
Nickel	1.93-3.32	2.43-3.32
Chrome	0.94-1.86	1.29-1.86
Molybdenum	0.17-0.63	0.27-0.63
Vanadium	< 0.03	< 0.03
Titanium	< 0.02	< 0.02
Copper	< 0.25	< 0.25
Arsenic	< 0.025	< 0.025
Tin	< 0.030	< 0.030
Antimony	< 0.025	< 0.025

FIGURE 6

IRON–CARBON PHASE DIAGRAM

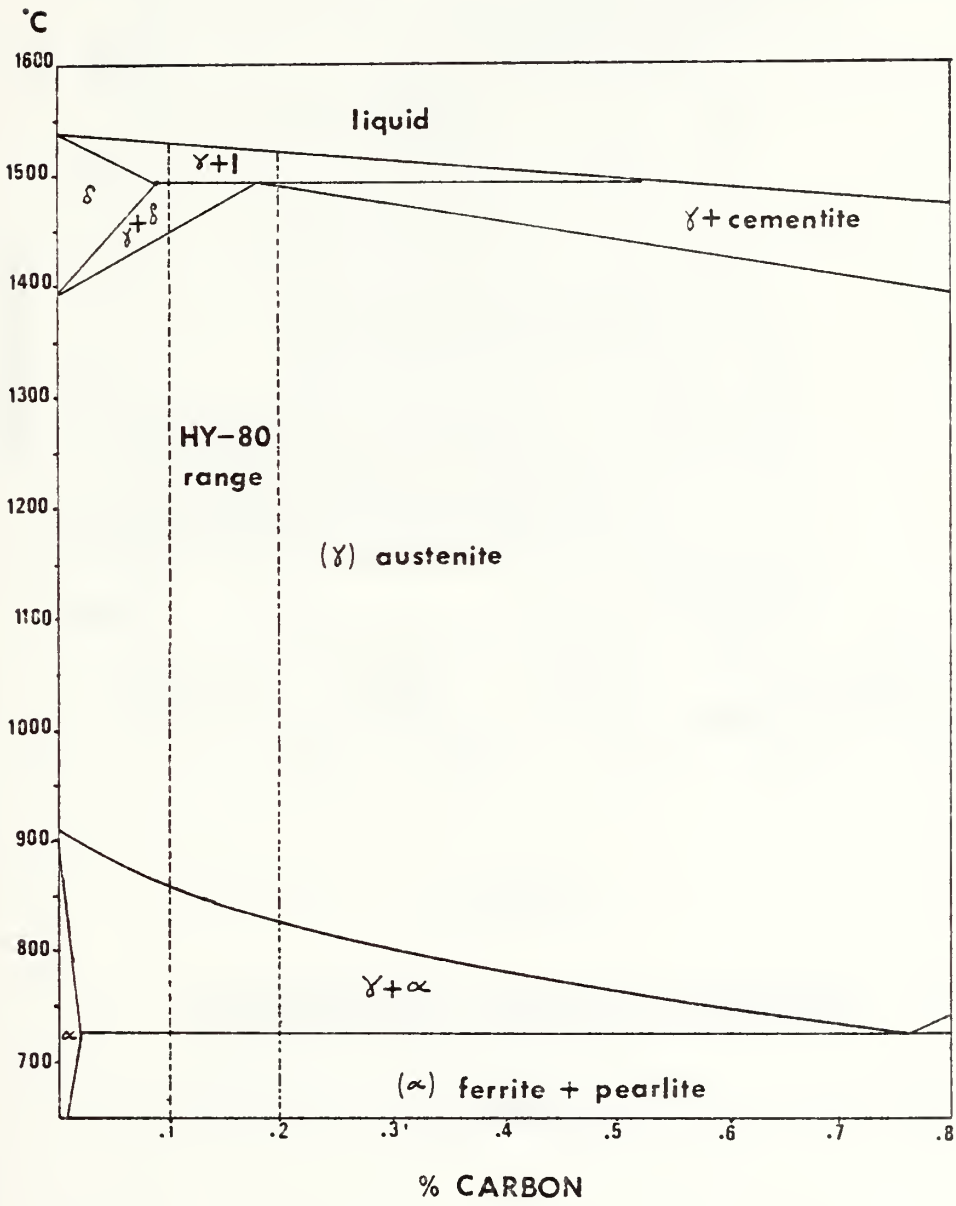

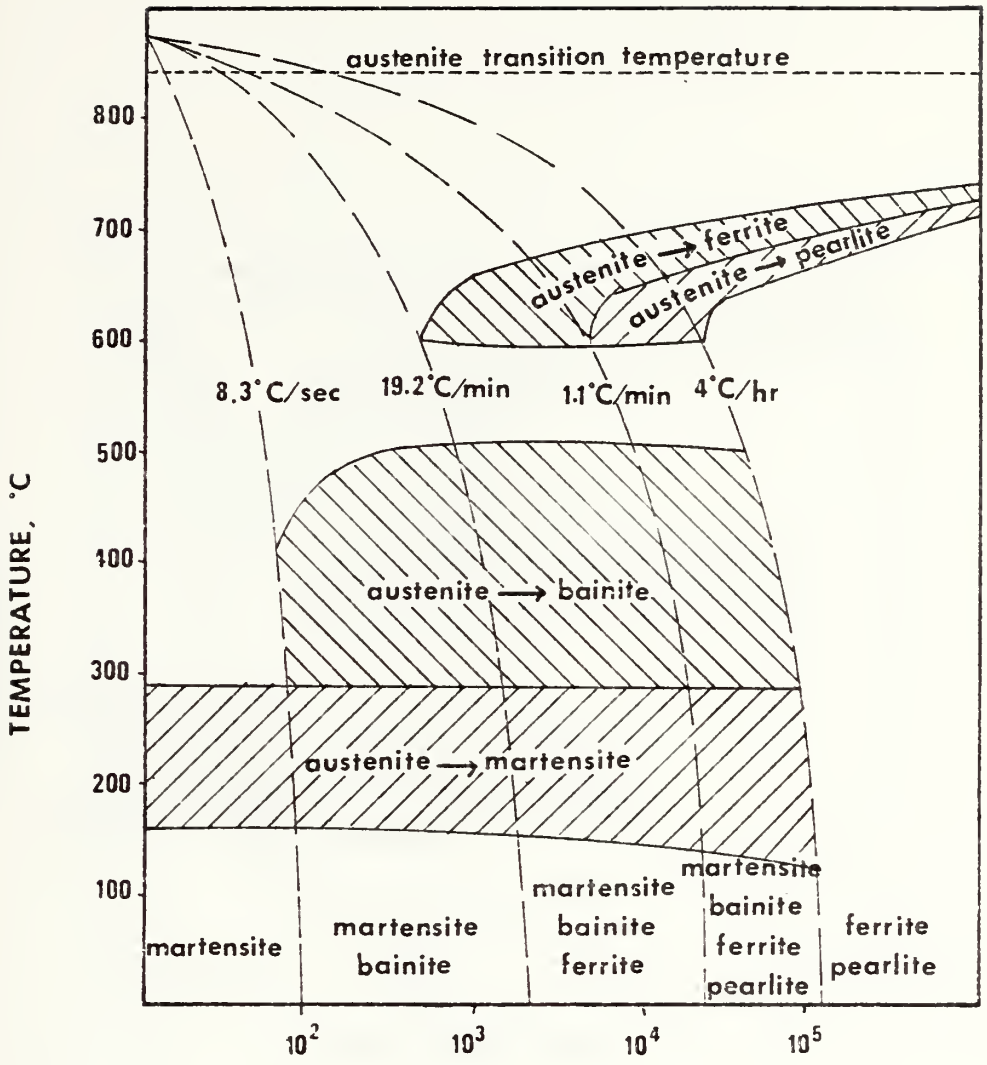

CONTINUOUS COOLING DIAGRAM

FIGURE 7

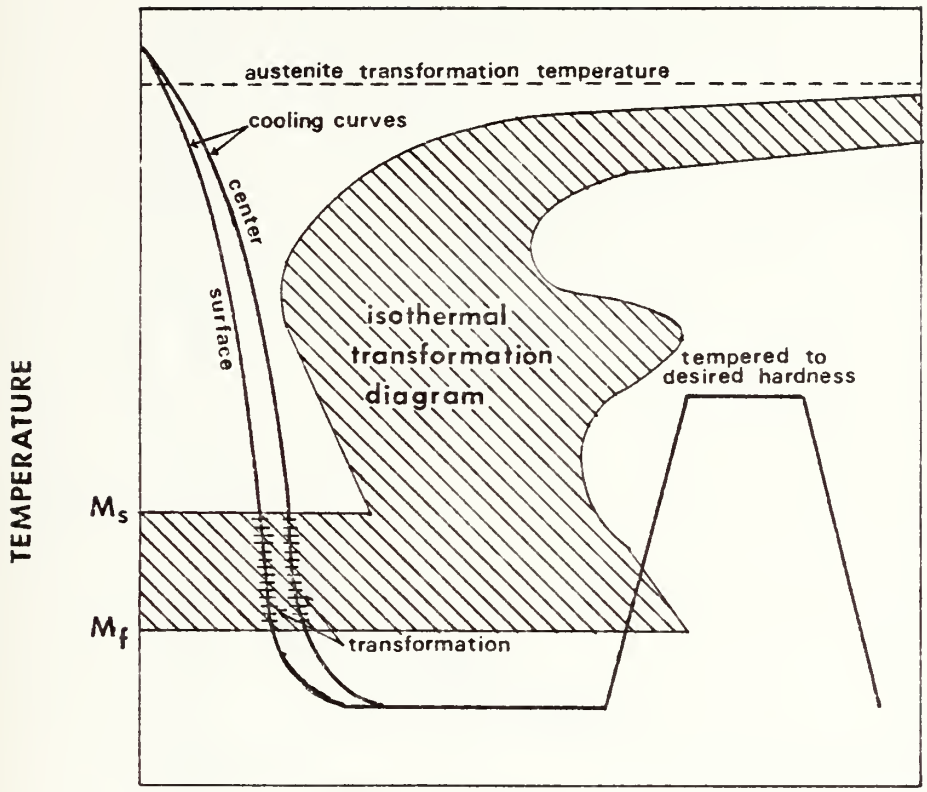

FIGURE 8

SCHEMATIC TRANSFORMATION
DIAGRAM FOR QUENCHING AND
TEMPERING TO TEMPERED MARTENSITE

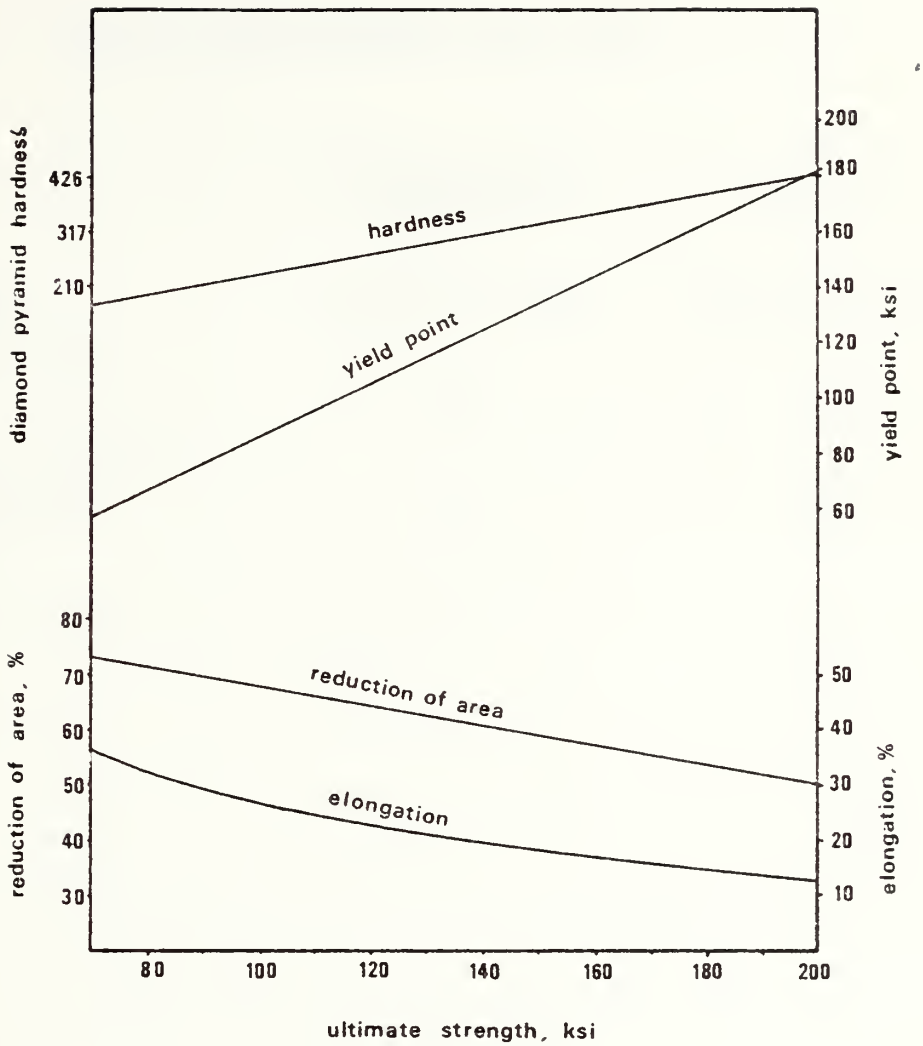

FIGURE 9

PHYSICAL PROPERTIES OF

TEMPERED MARTENSITE

TABLE 4

DUCTILE REQUIREMENTS FOR HY-80

	3/4 inch thick and under	over 3/4 inch
Yield Strength 0.2% offset, psi	80,000-100,000	80,000-99,500
Elongation 2 inches minimum, %	19	20
Reduction of Area minimum, %	--	50

4. METALLOGRAPHY OF THE BENT PLATES

Samples were cut from the beam paths of the bent plates as shown in Figure 10 and mounted for metallographic examination.

Transverse sections through the centerline and edge of the heat affected zone were polished and etched with nitol. Picral was found to be ineffective, probably because of the high concentration of chrome in this alloy.

The heat affected area of the sections were clearly visible in all etched samples. The characteristic banding of the plates, mentioned in an earlier citation, was also evident. This banding was darkest at the center of the thickness of the plates. Under 1000x magnification the area had many pits and spherical precipitates. This was common to all the plates, including the controls, and is not an effect of the laser bending process.

The samples from Plate 2 had the largest area of visible damage. Examination at 40x revealed three distinct zones of microstructure. Zone 1 was an area of greatly enlarged grains immediately adjacent to the irradiated edge. This is the upper region in Figure 11. Zone 2 was an area of dark, dense precipitate arranged in bands or streaks. It starts at the bottom of Figure 11 and extends through the top half of Figure 12. The bottom of Figure 12 is the unaffected

baseplate. It has the uniform grain of HY-80 that has been properly heat-treated. This was assigned Zone 3. Figure 13 is a microphotograph from the opposite edge of the section, taken at the same magnification. The structure is fine-grained tempered martensite.

Examination of the irradiated edge of Plate 2 at 1000x, Figure 14, reveals that the surface layer of grains may have approached the melting point. The internal structure of the grains is disorganized, the upper surface rounded. Note that the plates were sandblasted, which may have contributed to the shape of the surface. But Figure 19, which is the irradiatated edge of Plate 1, shows no rounding.

Figure 15 is a representative view of the structure in Zone 1 of Plate 2 at 1000x. It shows extremely large grains of martensite. The grain size of martensite is determined by the grain size of the austenite from which it is made. After the temperature exceeds the austenite transition temperature, the higher into the austenite region the sample reaches before cooling, the larger the resultant martensite grain size. The large grain size in this area confirms the nearly fused appearance of the surface and the estimated peak surface temperature in Table 2.

For most of Zone 2, the carbide precipitate is so thick that it completely obscures any underlying structure. This region is basically an area of over-tempering. The same

process that is used to temper martensite, the precipitation of spherical carbides, is here carried to the extreme. This is probably the region that spends the longest time in the temperature zone that is "forbidden" by the HY-80 specifcation to avoid temper embrittlement.

At the bottom of Zone 2, the precipitation thins out into bands. Figure 16 is a photomicrograph of the mixed region. The streaks of precipitate resolve themselves into spherical clumps of fine spherical carbide bodies distributed through the normal tempered martensite structure. Presumably, there is a decreasing gradation in grain size in the underlying martensite throughout Zone 2. The bottom of Zone 2 marks the end of the visible heat affected zone.

Figure 17 is the structure of the unaffected plate at 1000x. Comparison with Figure 15 shows how much the structure of the plate was changed.

Figure 18 shows the irradiated edge of Plate 3. This plate did not reach as high a surface temperature as Plate 2. But the surface does show a similar rounding. The grains of martensite are enlarged, but not as much as in Plate 2. This sample also has masses of carbide precipitate within the grains, unlike those in Figure 15. Zones 2 and 3 were essentially identical to those zones in plate 2.

In the sample from Plate 1, which received the lowest heat input, there is no visible grain growth. Zone 1 is

discernible by its lack of carbide precipitate. As can be seen in Figure 19 at 1000x, it is astonishingly fine-grained, even finer than the unheated plate. This suggests that it was heated to just inside the austenite region before cooling.

Zone 2 is largely the same in appearance as in the previous plates. Figure 20 is a photograph of the mixed region of Plate 1, that shows very clearly the spherical masses of precipitate.

The samples from Plates 4 and 5 were similar to Plate 1 in appearance.

Table 5 contains the depth of Zone 1 and Zone 2 at the centerline of the heat affected zone for each plate.

Figure 21 is a plot of the depth of the visible damage versus the half-angle of the bend. Figure 22 is a plot of the depth of visible damage versus the heat input. There is a clear correlation between the method of bending and the depth of damage. For the same degree of bend, a multiple pass method does much less damage to the plate than a single pass method.

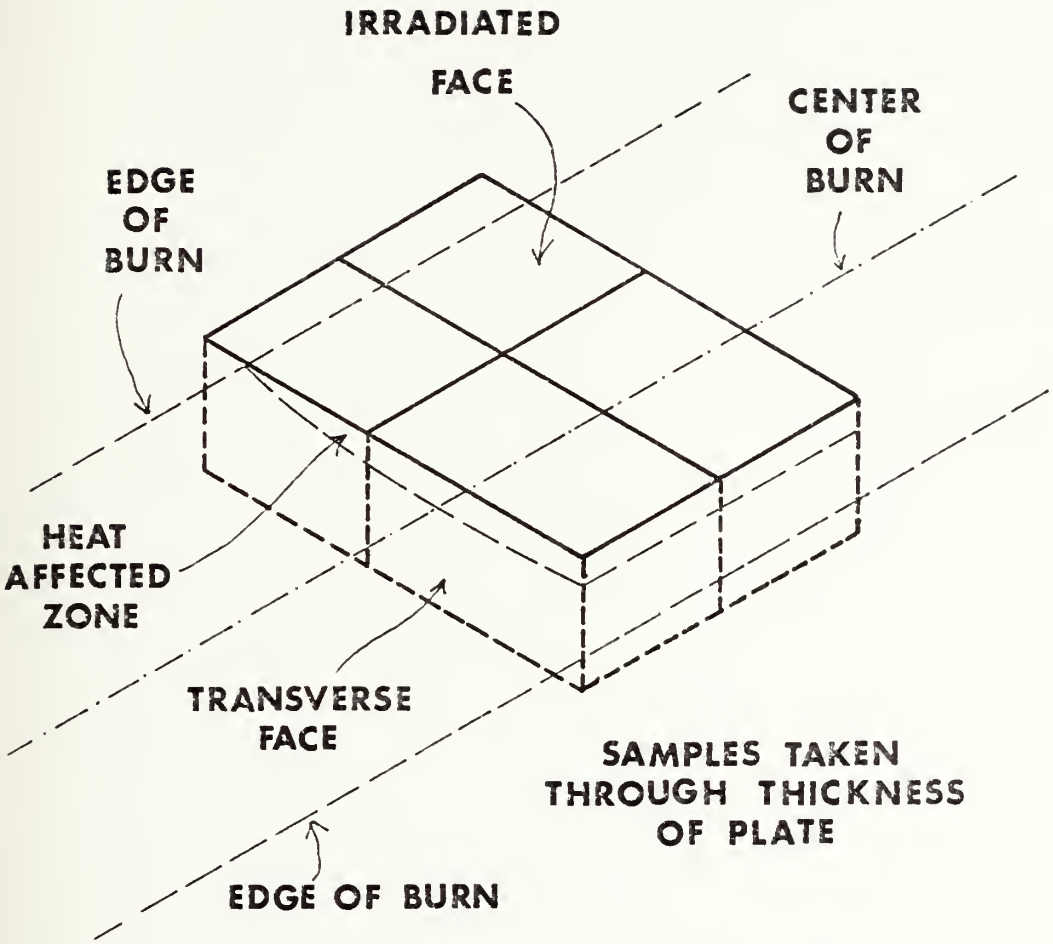

DIAGRAM OF METALLOGRAPHIC SAMPLES

FIGURE 10

FIGURE 11

PLATE 2 IRRADIATED EDGE 40X

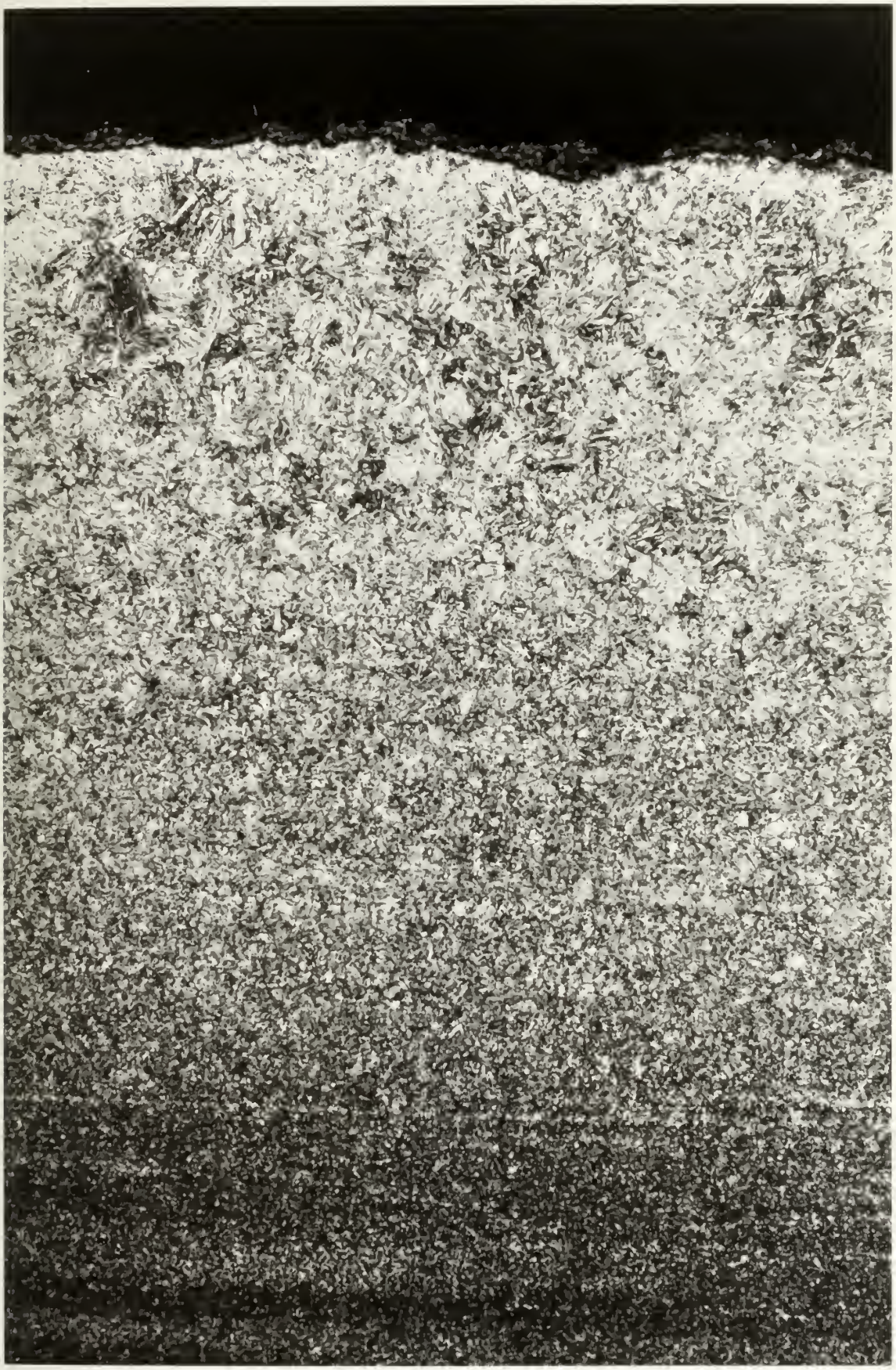

FIGURE 12

PLATE 2 BOTTOM OF HEAT AFFECTED ZONE 40X

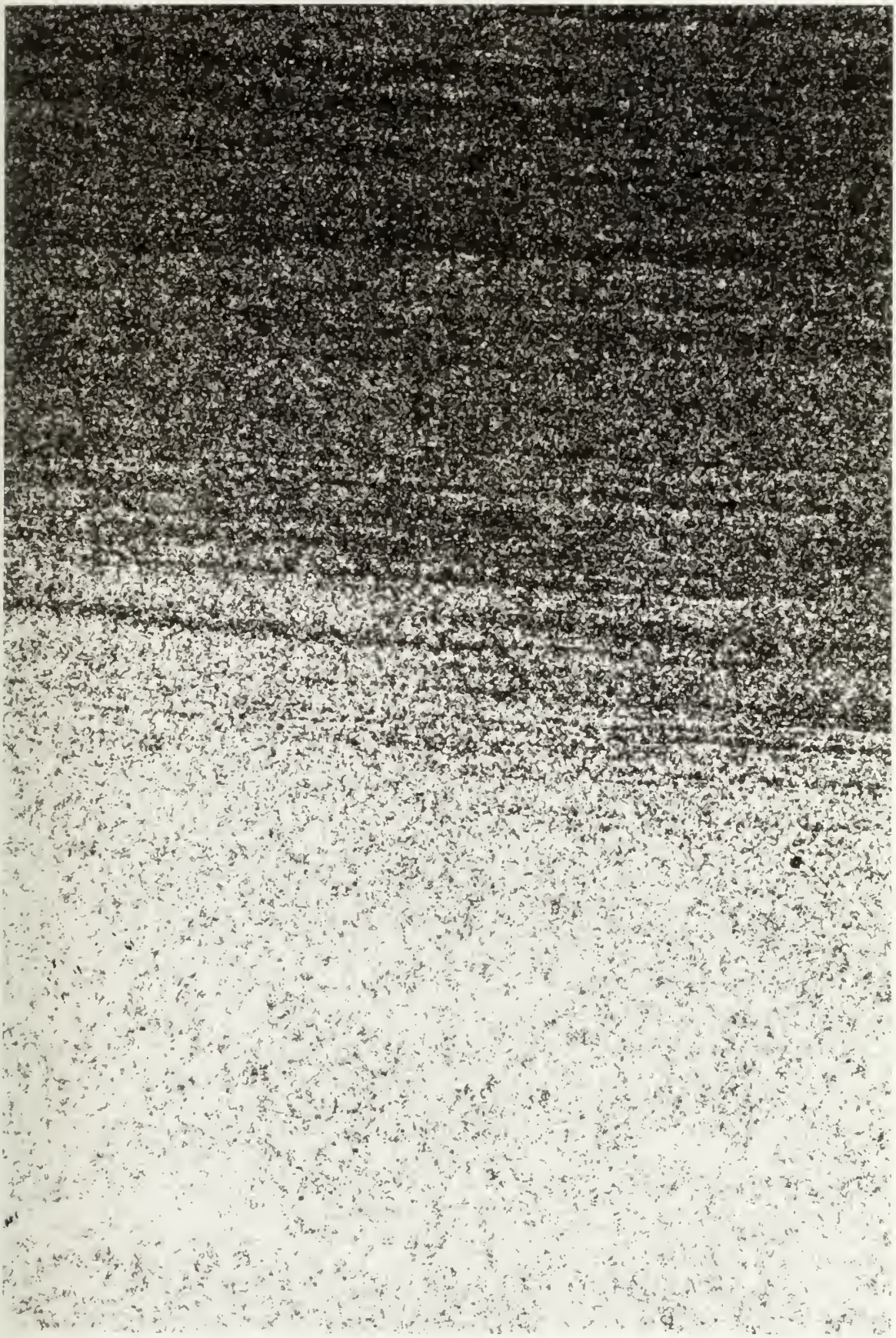

FIGURE 13

PLATE 2 UNAFFECTED BASEPLATE 40X

FIGURE 14

PLATE 2 IRRADIATED EDGE 1000X

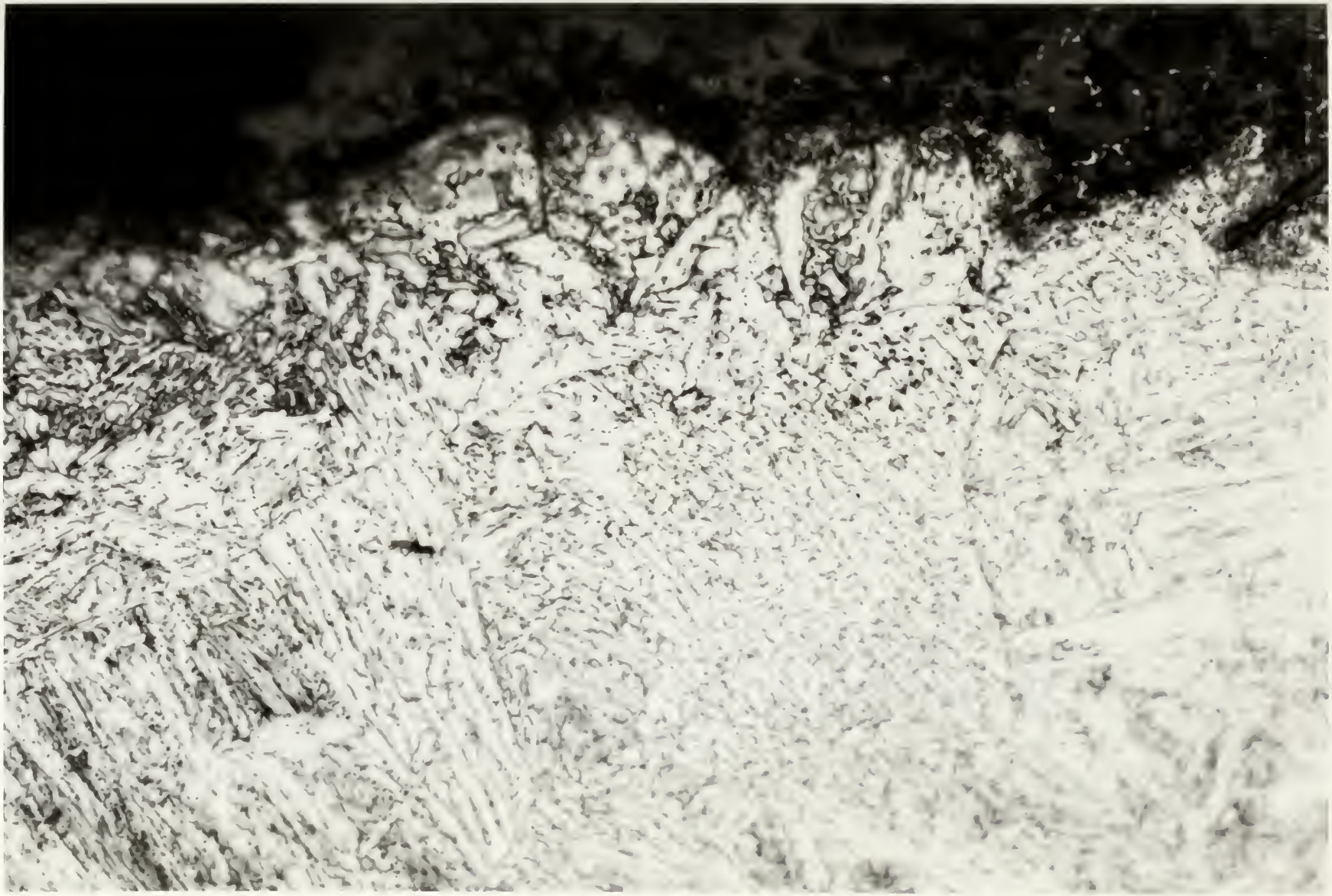

FIGURE 15

PLATE 2 ZONE 1 1000X

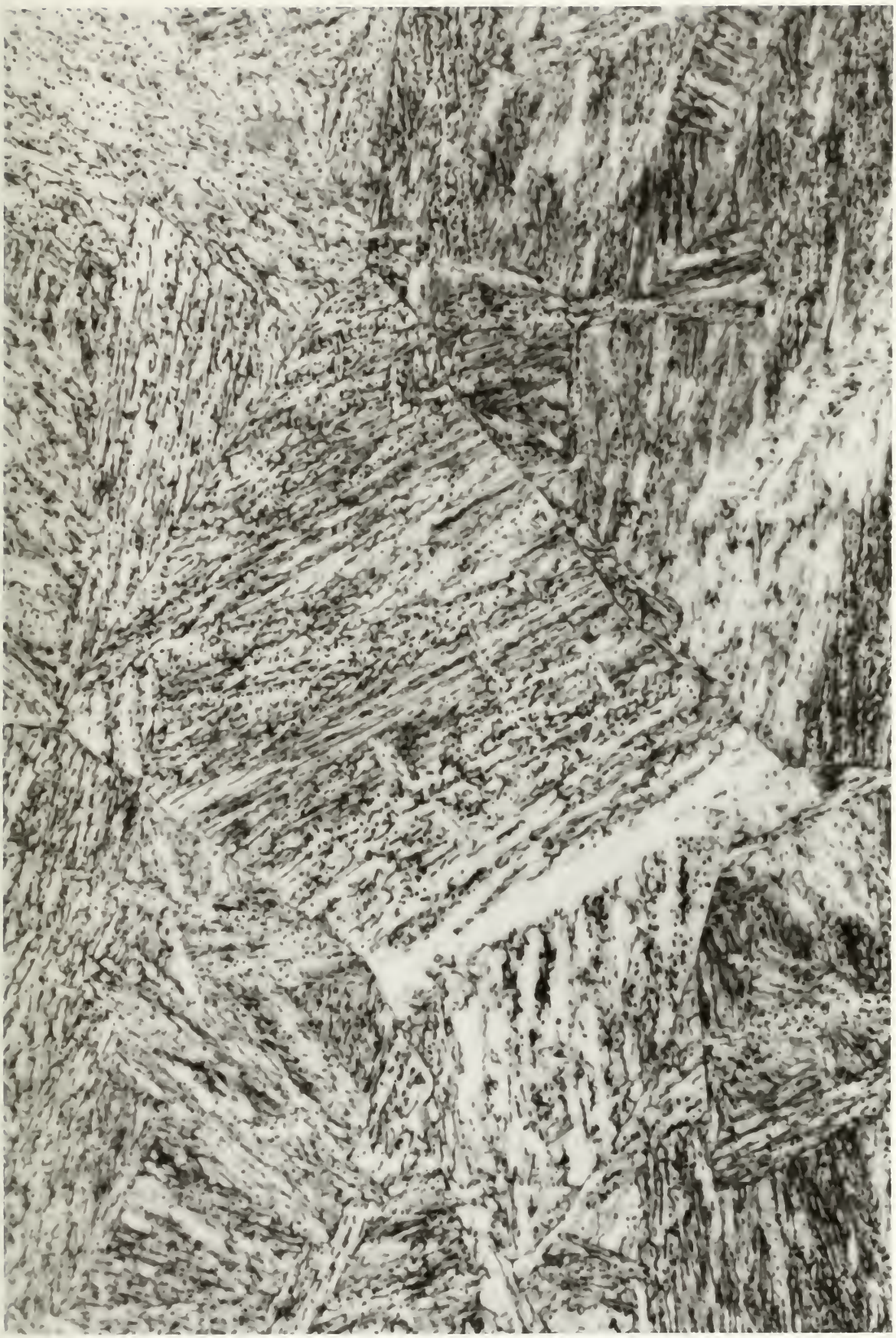

FIGURE 16

PLATE 2 MIXED REGION 1000X

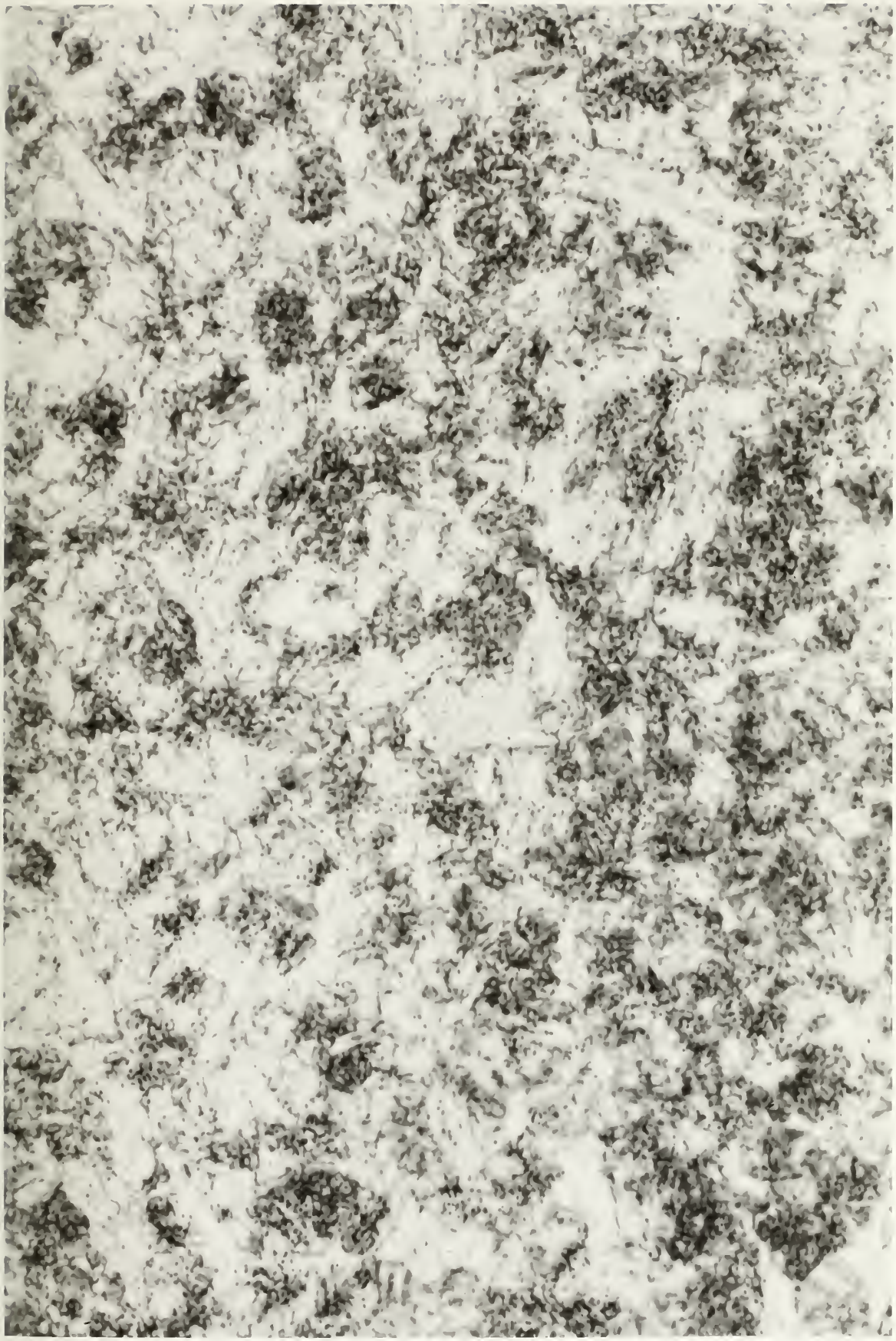

FIGURE 17

PLATE 2 UNAFFECTED BASEPLATE 1000X

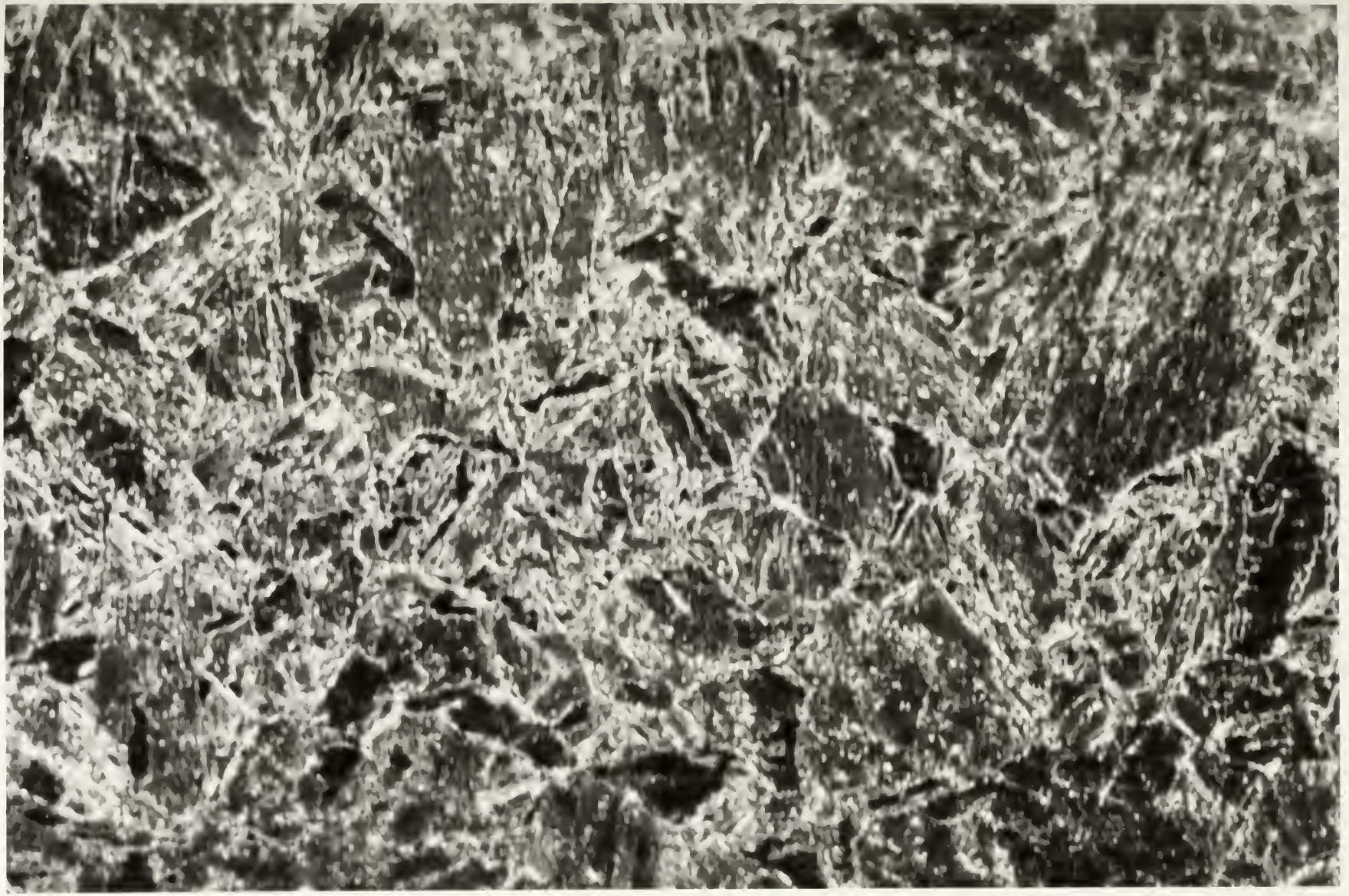

FIGURE 18

PLATE 3 IRRADIATED EDGE 1000X

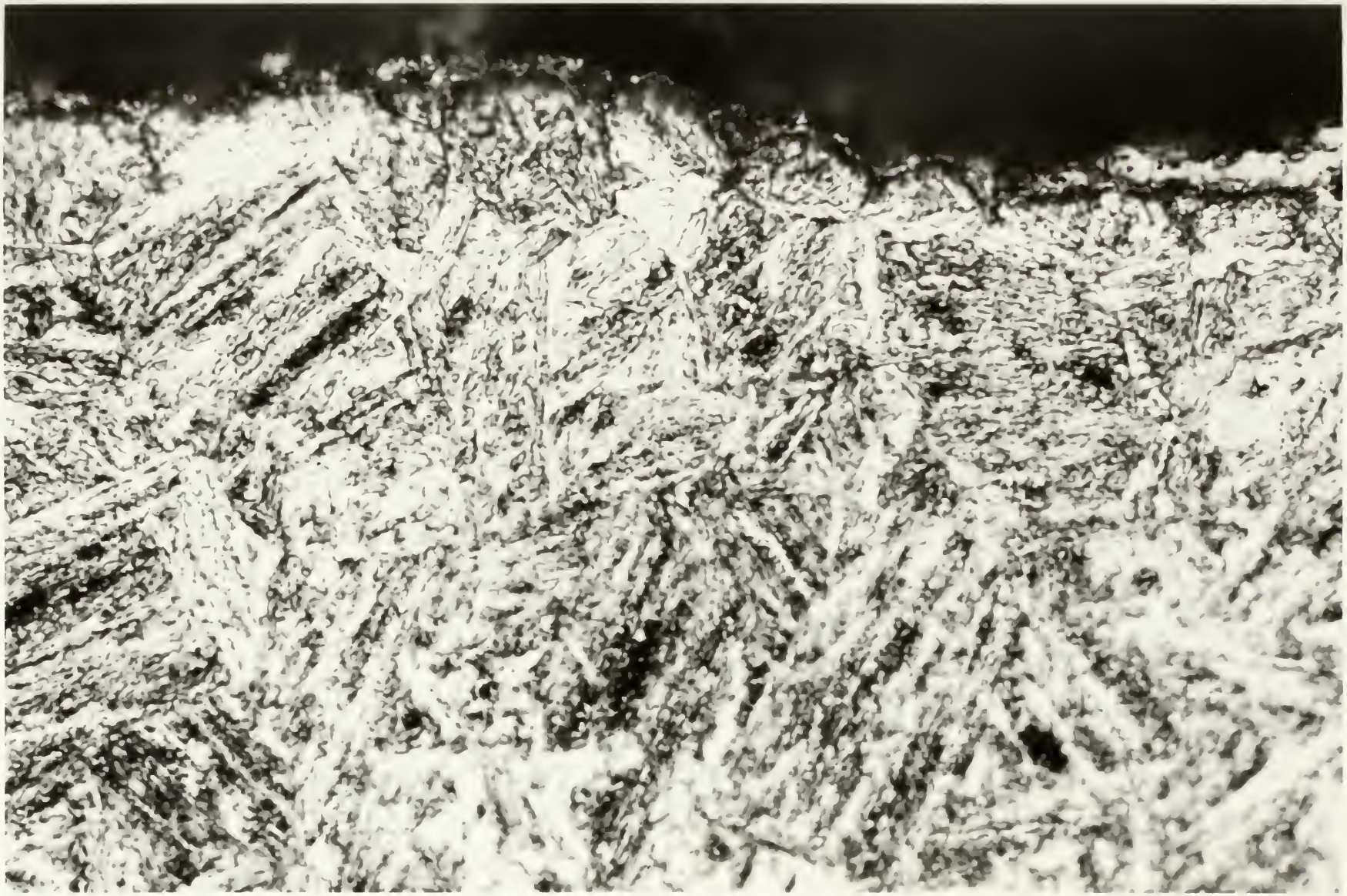

FIGURE 19

PLATE 1 IRRADIATED EDGE 1000X

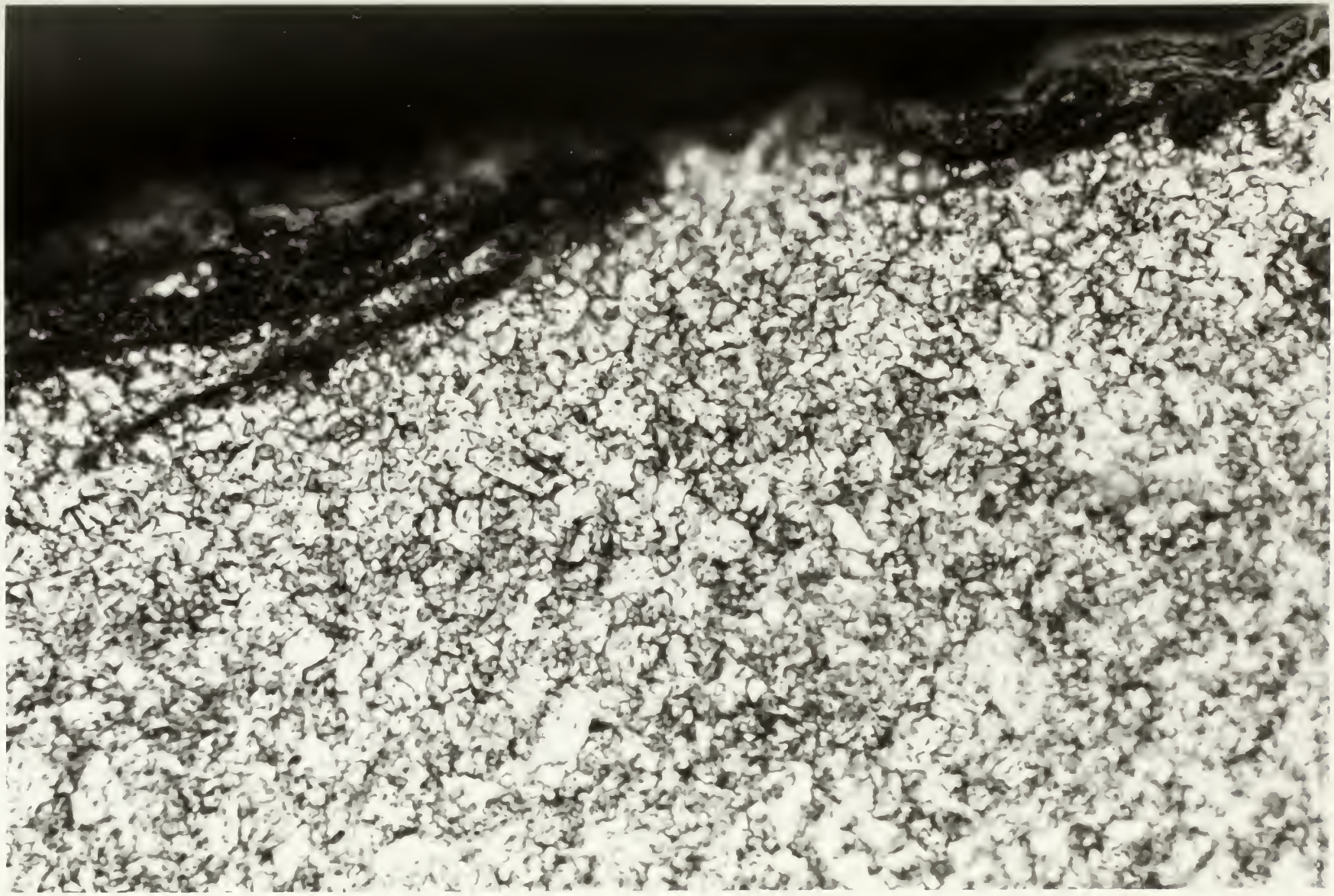

FIGURE 20

PLATE 1 MIXED REGION 1000X

TABLE 5

DEPTH OF VISIBLE DAMAGE

Plate Number	Depth of Zone 1 [mm]	Depth of Zone 2 [mm]	Total Depth [mm]
1	0.1	1.3	1.4
2	3.5	3.5	7.0
3	1.1	2.3	3.4
4	0.1	2.0	2.1
5	0.1	1.8	1.9

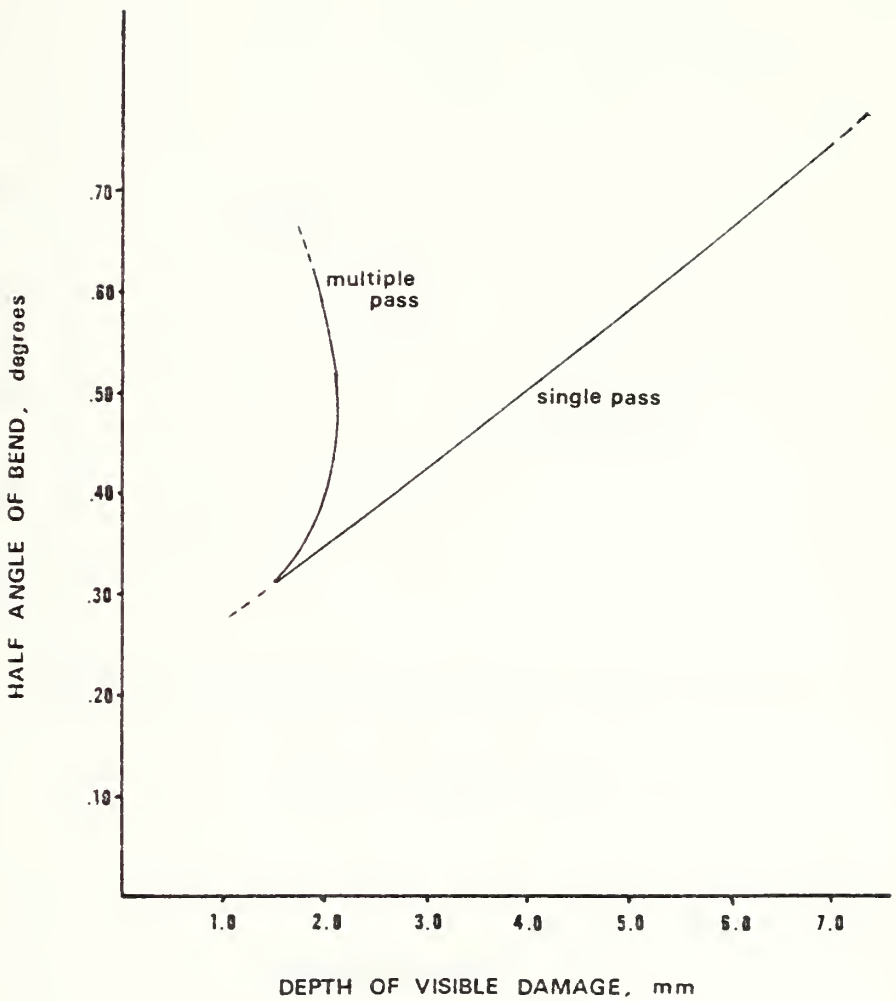
HALF ANGLE OF BEND, degrees
.70
.60
.50
.40
.30
.20
.10
multiple pass
single pass
1.0
2.0
3.0
4.0
5.0
6.0
7.0
DEPTH OF VISIBLE DAMAGE, mm

FIGURE 21

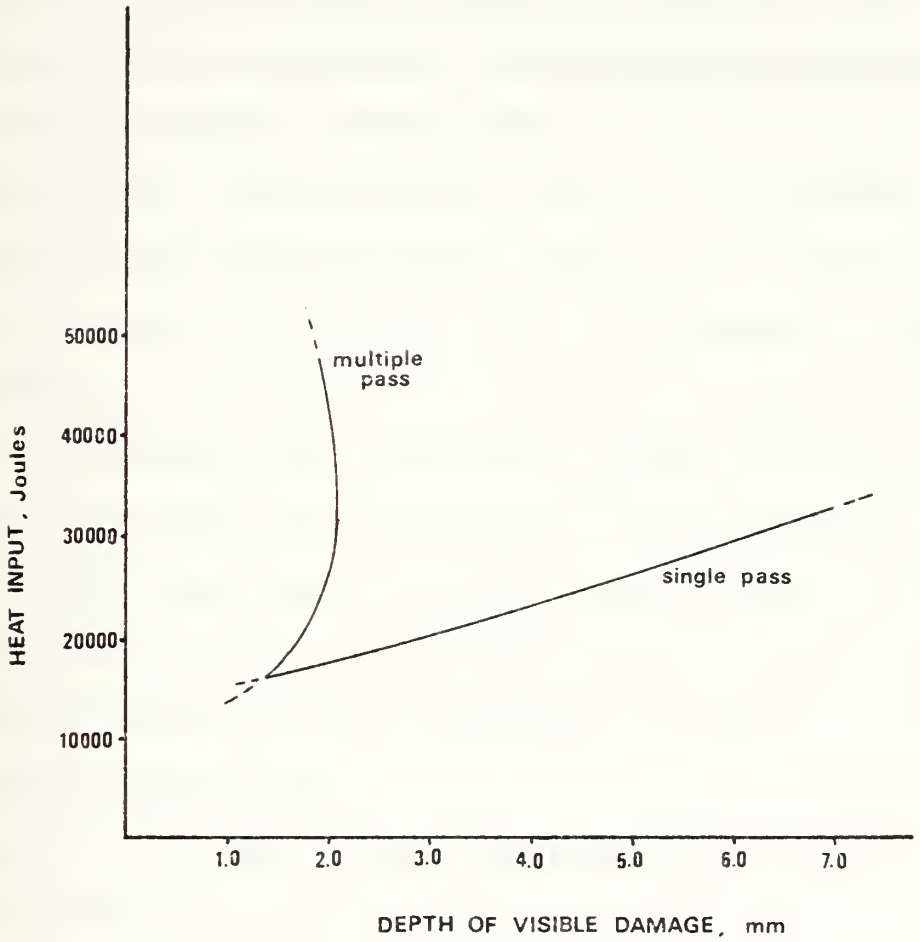
HEAT INPUT, Joules
50000
40000
30000
20000
10000
multiple pass
single pass
1.0
2.0
3.0
4.0
5.0
6.0
7.0
DEPTH OF VISIBLE DAMAGE, mm

FIGURE 22

5. MICROHARDNESS EXAMINATION OF THE BENT PLATES

The transverse sections through the beam-path centerline were polished to remove the etched surface and prepare them for microhardness measurements. Measurements were made on a LECO DM-400 Hardness Tester using the Vickers or diamond pyramid method. This device has a microprocessor for calculating the hardness value. Therefore, the data is reported directly in DPH rather than in diagonals. Hardness measurements were taken in a line into the depth of each plate. Measurements were continued through the entire depth of Plate 2 to establish a baseline for the unaffected plate area. On the other plates, the line was extended only until the baseplate material had definitely been reached, based on the visible depth of Zone 2 previously measured, and the established expected DPH.

Tables 6-10 are the hardness measurements for each plate.

Figure 23 is a plot of hardness versus depth for the plates that were bent in a single pass. The maximum measured hardness was 430 DPH on Plate 2, which received the highest heat input. In general, the hardness is directly proportional to the heat input. The depth of the hardened zone corresponds well with the depth of visible damage. The hardest area in each case appears near, but not at the irradiated surface.

Figure 24 is a plot of hardness versus depth of the

plates that were bent with multiple passes. The maximum measured hardness was 440 DPH, higher than Plate 2. The depth of the hardened zone again corresponds with the depth of visible damage. The hardened depth is much smaller for the mutliple pass plates than for the single pass plates.

The hardness values measured near the irradiated surface are consistent with the hardness range for untempered martensite[34].

Samples from Plate 2 were mounted with the irradiated surface exposed. Measurements were made of the surface hardness from the baseplate outside the heat affected zone to the centerline of the beam burn. The surface was very irregular with voids, hills and visible surface micro-cracks. This introduces a large degree of uncertainty to the measurements as it was difficult to obtain a clear diamond imprint is some areas. Table 11 is a summary of the data and Figure 25 is a plot of the hardness versus the distance from the edge of the heat affected zone to the centerline of the burn. The shape of the plot is roughly consistent with the familiar plot of hardness across a weld, although large local swings in the hardness value are evident.

TABLE 6

MICROHARDNESS OF PLATE 1

Depth [mm]	Hardness [DPH]
0.076	313.3
0.253	313.8
0.452	334.4
0.654	355.7
0.851	295.1
1.055	247.5
1.263	243.9
1.473	232.4
1.673	228.5
1.877	236.6
2.088	239.6
2.296	244.3
2.499	243.9
2.705	238.5
2.909	235.8
3.120	227.0
3.322	235.0
3.548	244.3
3.757	233.6
3.988	233.9

TABLE 7

MICROHARDNESS OF PLATE 2

Depth [mm]	Hardness [DPH]
0.068	284.8
0.104	318.5
0.290	380.7
0.420	402.4
0.498	429.7
0.625	384.5
0.710	405.7
0.829	370.8
0.912	372.3
1.033	357.1
1.115	398.2
1.229	367.1
1.391	358.5
1.526	386.9
1.631	357.1
1.631	359.9
1.781	362.1
1.837	370.1
1.931	379.1
2.037	372.3

TABLE 7 (CONTINUED)

Depth [mm]	Hardness [DPH]
2.132	399.9
2.234	319.1
2.334	386.1
2.437	328.2
2.546	320.9
2.653	316.2
2.757	329.4
2.855	281.4
2.956	292.5
3.056	282.8
3.157	287.3
3.260	284.8
3.377	288.9
3.485	325.7
3.587	290.4
3.687	308.7
3.687	303.1
3.793	305.9
3.887	292.5
3.894	298.8
4.006	294.6

TABLE 7 (CONTINUED)

Depth [mm]	Hardness [DPH]
4.112	290.4
4.221	293.0
4.333	277.0
4.442	265.0
4.553	273.2
4.667	288.9
4.778	273.7
4.885	287.3
4.992	298.3
5.099	279.9
5.208	281.9
5.325	262.3
5.441	245.1
5.556	236.2
5.675	231.3
5.791	228.5
5.900	235.4
6.018	231.7
6.131	247.1
6.251	235.0
6.369	237.3

TABLE 7 (CONTINUED)

Depth [mm]	Hardness [DPH]
6.485	224.9
7.137	241.9
7.778	237.7
8.393	245.5
9.245	243.5
10.526	244.7
11.173	251.6
11.785	254.9
12.403	241.2
13.010	250.8
13.322	245.1

TABLE 8

MICROHARDNESS OF PLATE 3

Depth [mm]	Hardness [DPH]
0.096	402.3
0.202	410.5
0.309	417.8
0.411	397.7
0.514	417.8
0.616	384.2
0.715	409.3
0.816	402.2
0.919	363.8
1.017	405.7
1.120	350.6
1.216	326.3
1.316	323.7
1.423	343.9
1.522	355.8
1.626	322.1
1.735	307.0
1.838	322.1
1.942	330.7
2.054	339.6

TABLE 8 (CONTINUED)

Depth [mm]	Hardness [DPH]
2.166	326.3
2.280	320.9
2.388	306.5
2.500	299.9
2.612	303.7
2.721	281.4
2.832	279.4
2.933	272.7
3.039	274.1
3.145	289.4
3.252	282.8
3.356	278.4
3.460	252.8
3.563	227.0
3.670	225.6
3.777	233.6
3.880	226.0
3.988	236.2
4.095	234.3
4.197	235.0
4.305	239.6
4.405	227.7
4.517	232.1

TABLE 9

MICROHARDNESS OF PLATE 4

Depth [mm]	Hardness [DPH]
0.063	355.0
0.095	378.4
0.124	387.7
0.228	390.1
0.328	426.9
0.419	376.1
0.521	403.2
0.617	373.1
0.713	361.4
0.819	337.6
0.920	352.3
1.023	347.5
1.123	316.2
1.222	353.0
1.328	349.5
1.425	362.8
1.531	331.3
1.644	353.6
1.756	313.3
1.864	291.9
1.983	265.0

TABLE 9 (CONTINUED)

Depth [mm]	Hardness [DPH]
2.086	241.9
2.188	246.3
2.291	256.2
2.409	252.0
2.524	243.9
2.635	234.7
2.751	243.5
2.855	249.9
2.964	259.2
3.069	251.2
3.171	235.8

TABLE 10

MICROHARDNESS OF PLATE 5

Depth [mm]	Hardness [DPH]
0.071	413.5
0.172	424.2
0.269	439.1
0.365	421.5
0.460	428.8
0.559	386.9
0.657	386.1
0.754	383.8
0.856	372.3
0.956	384.5
1.051	387.7
1.149	393.3
1.248	351.6
1.339	369.3
1.438	351.6
1.537	347.5
1.630	345.5
1.732	348.9
1.830	304.2
1.937	264.5
2.039	241.2

TABLE 10 (CONTINUED)

Depth [mm]	Hardness [DPH]
2.141	238.8
2.247	235.8

TABLE 11

SURFACE HARDNESS ON PLATE 2

Distance [mm]	Hardness [DPH]
baseplate	129.2
baseplate	90.3
baseplate	162.4
baseplate average	127.0
0.00	204.7
1.00	210.2
2.00	337.6
2.57	178.8
3.12	357.1
4.12	583.8
5.68	391.7
7.00	592.7
7.76	756.8
8.74	735.7
9.84	604.9
10.84	375.3
13.27	477.7
14.44	432.8
15.28	951.3
17.18	515.1
20.37	576.8
21.00	471.6

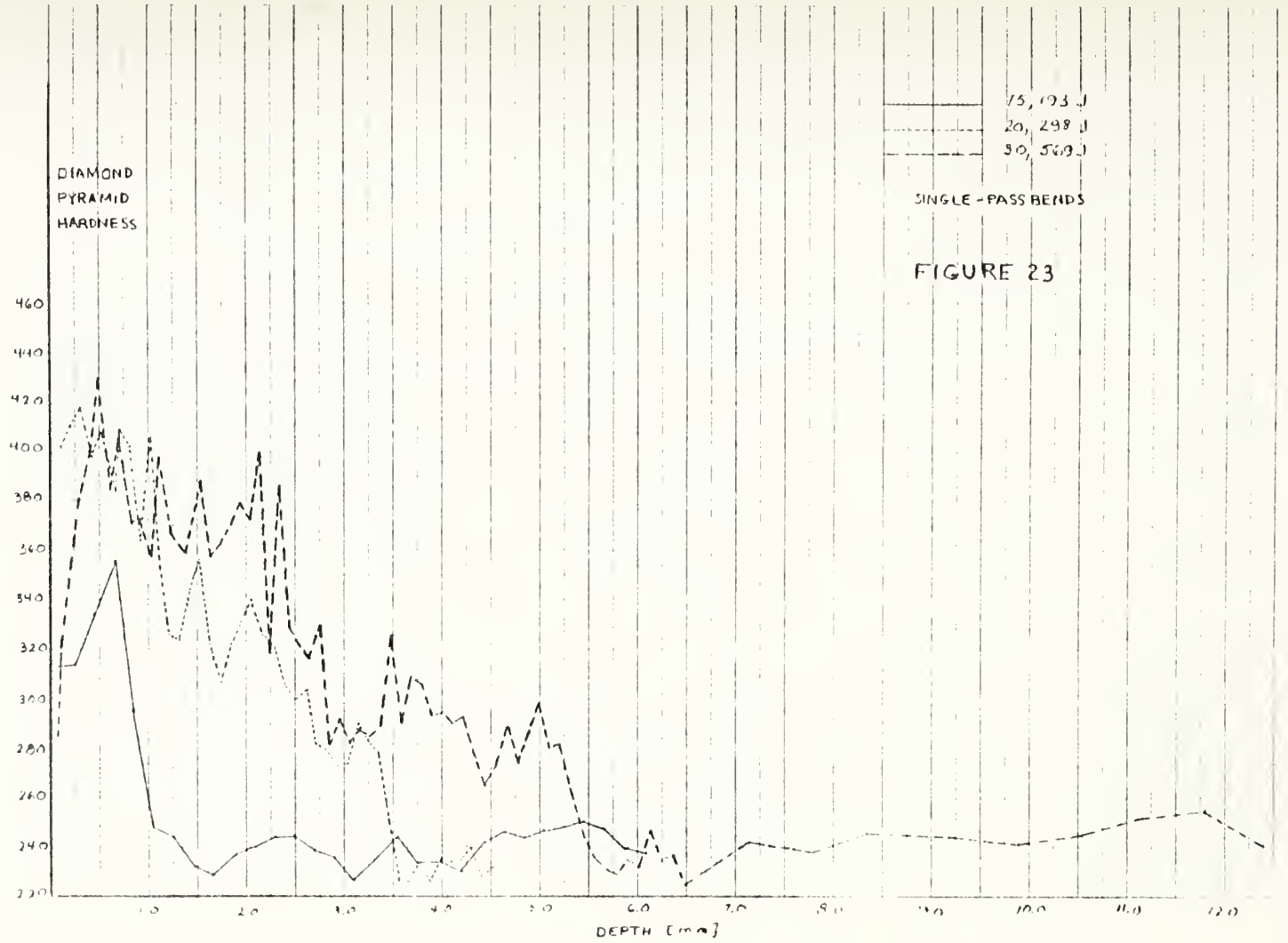
DIAMOND
PYRAMID
HARDNESS
460
440
420
400
380
360
340
320
300
280
260
240
220
DEPTH [mm]
15, 193 J
20, 298 J
30, 569 J
SINGLE-PASS BENDS

FIGURE 23

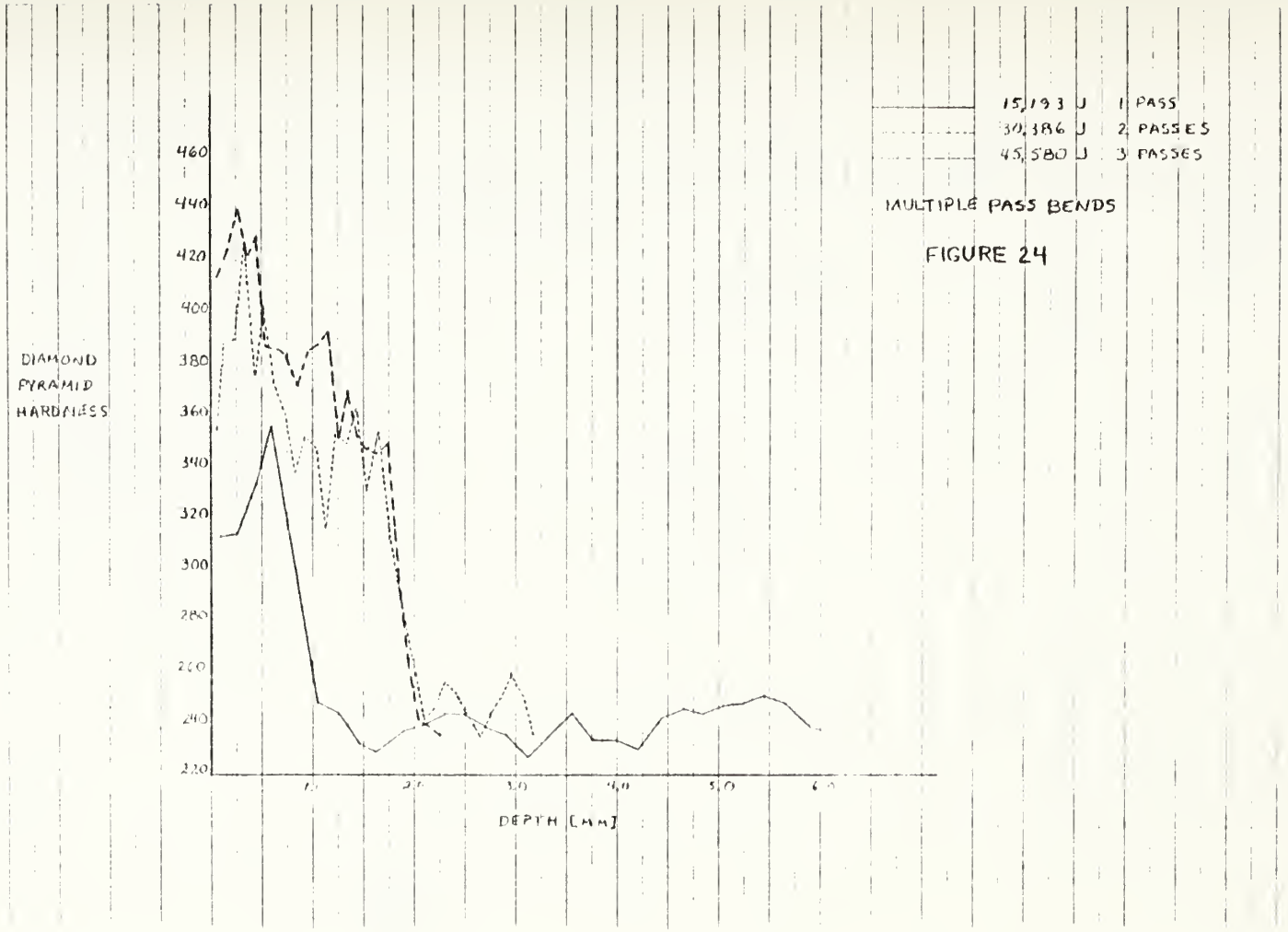
15,193 J 1 PASS
30,386 J 2 PASSES
45,580 J 3 PASSES
MULTIPLE PASS BENDS
DIAMOND PYRAMID HARDNESS
460
440
420
400
380
360
340
320
300
280
260
240
220
DEPTH [mm]

FIGURE 24

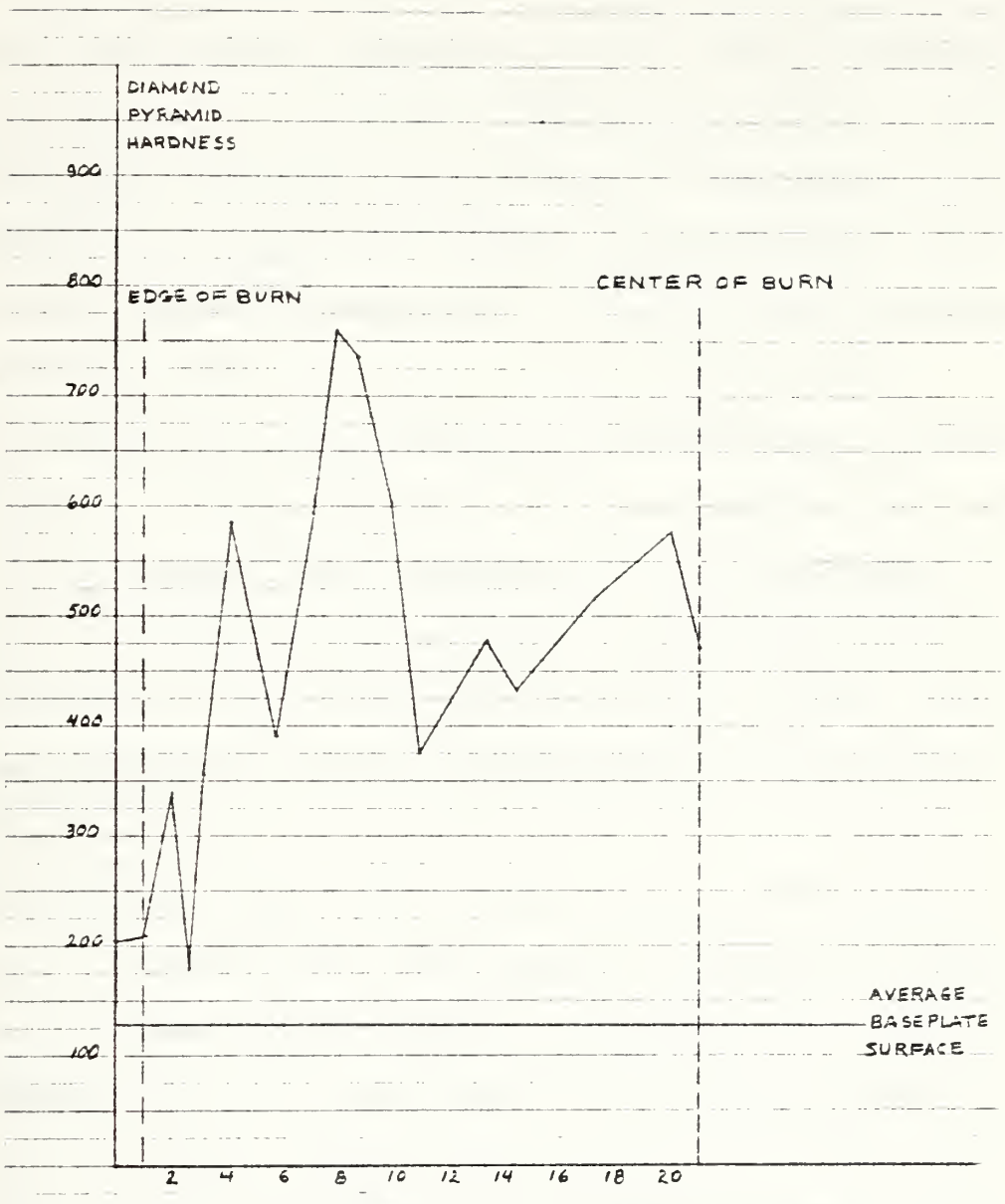

SURFACE HARDNESS OF PLATE 2

FIGURE 25

6. NOTCH TOUGHNESS OF THE BENT PLATES

The earliest plate received from the Naval Research Laboratory had two parallel burn lines on the surface. This plate had bent in an effort to determine if the basic idea was feasible. No data was recorded regarding laser power level, travel speed or beam size. The burn patterns were about two inches wide.

This plate was cut into reduced size Charpy bars as shown in Figure 26. One set of bars, L1, was notched at the center of the beam pattern. Another set, L2, was notched at the edge of the heat affected zone. A third set of bars were prepared from the center portion of the plate. This set served as controls, being outside the heat affected zone of the laser burns.

Two pieces were taken out of each line for metallographic examination. These pieces were mounted, polished, etched and examined under the microscope. It was found the the heat affected zones for these bends were very shallow, on the order of 0.6 mm. Therefore, the decision was made to place the notches normal to the irradiated surface so that at least some of the heat affected zone would contribute to the notch toughness behavior.

The finished bars were cooled with liquid nitrogen and dry ice. Initially, breaking the bars on a miniature Charpy machine was attempted. This was unsuccessful because the

force of the machine was too low. The samples were only slightly bent at a temperature of -40° C. Therefore, the tests were finally performed on a full scale Charpy machine.

Table 12 is a summary of the results of the Charpy tests.

Figures 27-29 are graphs showing the brittle-to-ductile transition for the control, the center of the beam path and the edge of the heat affected zone respectively. The results are summarized below:

Sample	Breaking Force Lower Shelf [ft-lbs]	Upper Shelf [ft-lbs]	Transition Temperature [°C]
Control	7	75	-54
Center of beam path	7	68	-50
Edge of beam path	9	78	-45

The above data would indicate a decrease in the upper shelf breaking force, or at least a flattening of the curve. More significantly, there appears to be a shifting of the ductile-to-brittle transition temperature to the right. This is a major consideration that indicates a deterioration of the toughness of the metal.

Visual examination of the fracture surfaces of the samples that were on the borderline between ductile and brittle revealed a slightly smaller shear lip on the edge

that was irradiated.

The method used for cooling the samples did not allow time for ensuring complete equilibration for the intermediate temperatures. This is reflected in the amount of scatter visible on the curves.

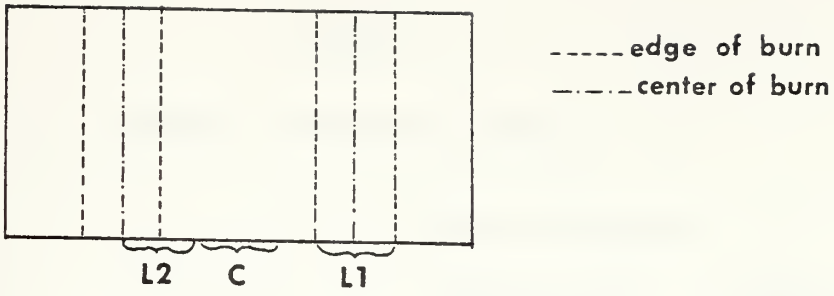

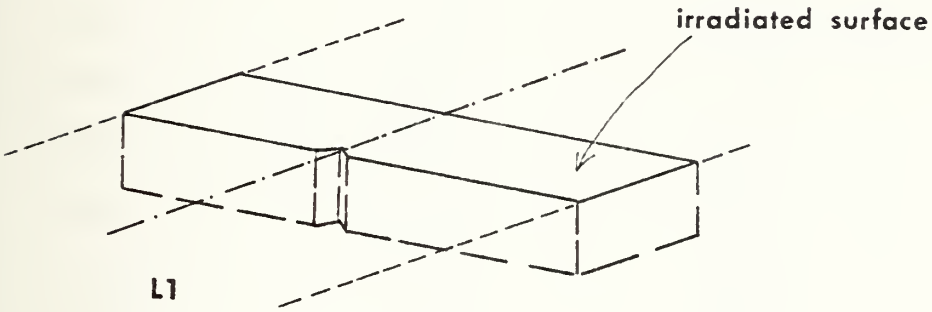

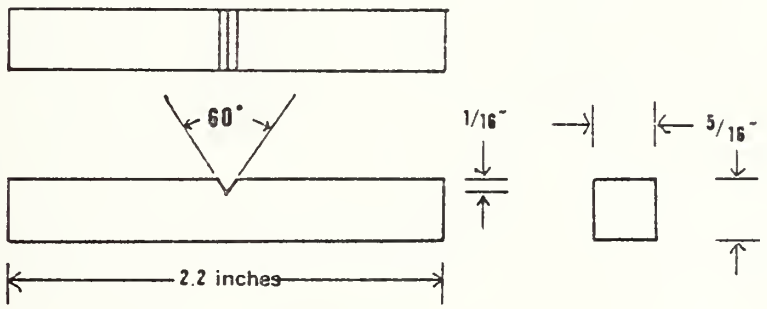

DIAGRAM OF CHARPY BARS

FIGURE 26

TABLE 12

SUMMARY OF CHARPY RESULTS

Temperature [C]	Force [ft-lbs] Control	Center of Beam Path	Edge of Beam Path
-210	7.0	7.0	9.0
-75	8.0	12.0	14.0
-60	20.0	8.0	19.0
-50	55.0	22.0	26.0
-45	72.0	66.0	70.0
-30	71.5	68.0	72.0
-30	66.0	58.0	58.0
-20	66.0	64.0	70.0
-15	72.0	70.0	70.0
-13	71.0	64.0	72.0
+20	73.5	66.0	76.0

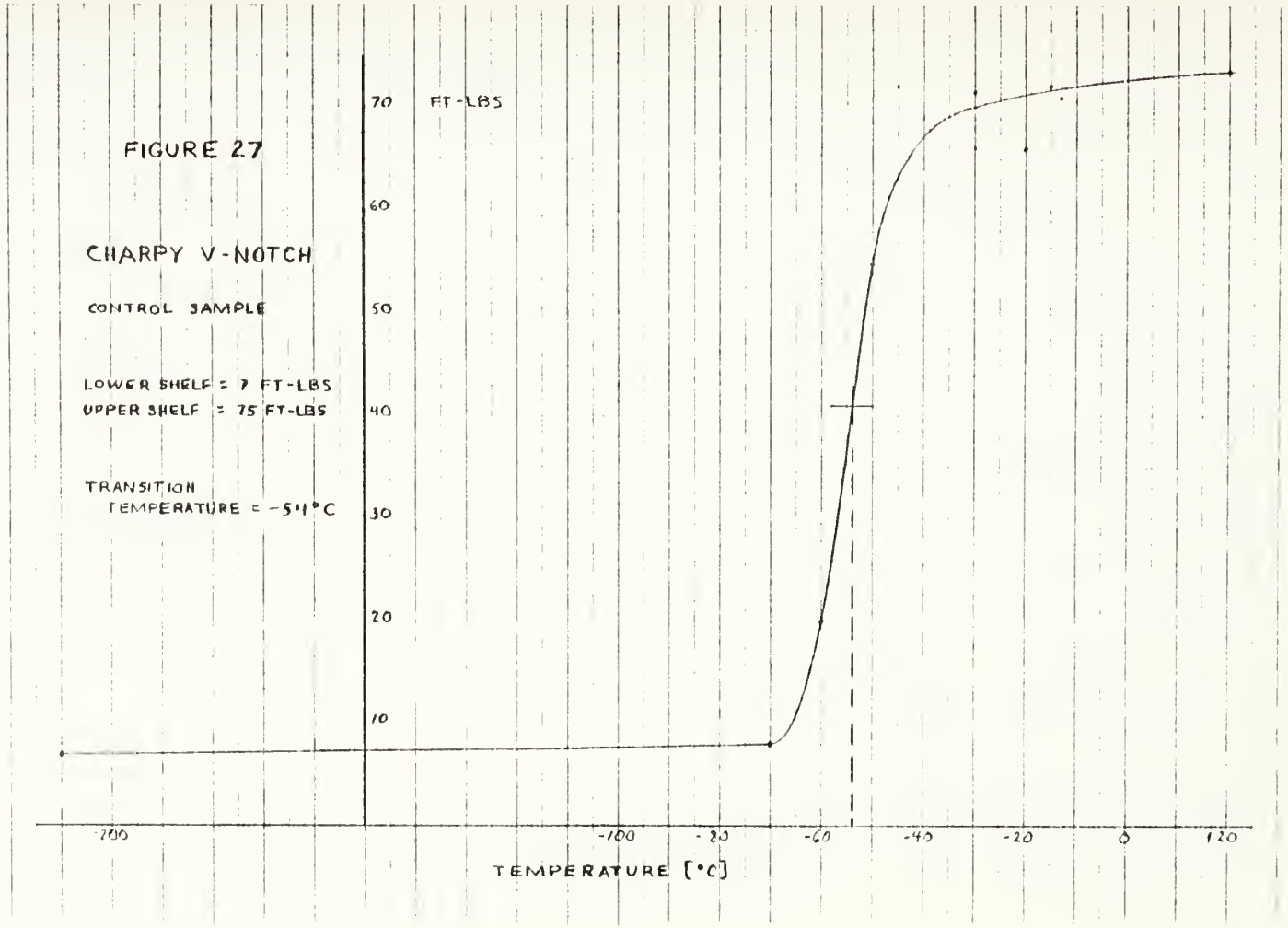
FIGURE 27
CHARPY V-NOTCH
CONTROL SAMPLE
LOWER SHELF = 7 FT-LBS
UPPER SHELF = 75 FT-LBS
TRANSITION TEMPERATURE = -54°C
70
60
50
40
30
20
10
FT-LBS
-100
-80
-60
-40
-20
0
120
TEMPERATURE [°C]

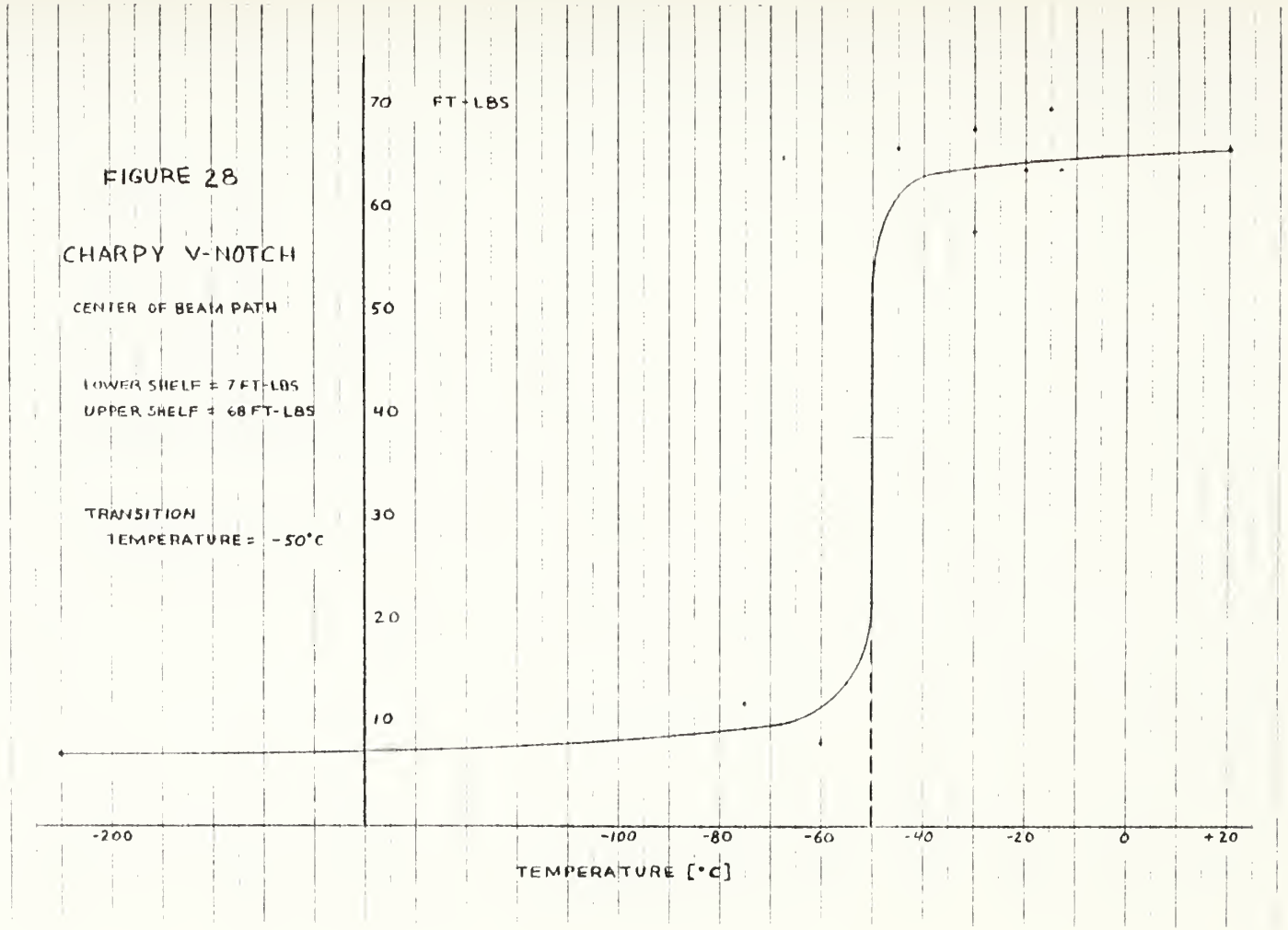
FIGURE 28
CHARPY V-NOTCH
CENTER OF BEAM PATH
LOWER SHELF = 7 FT-LBS
UPPER SHELF = 68 FT-LBS
TRANSITION TEMPERATURE = -50°C
70 FT-LBS
60
50
40
30
20
10
-200
-100
-80
-60
-40
-20
0
+20
TEMPERATURE [°C]

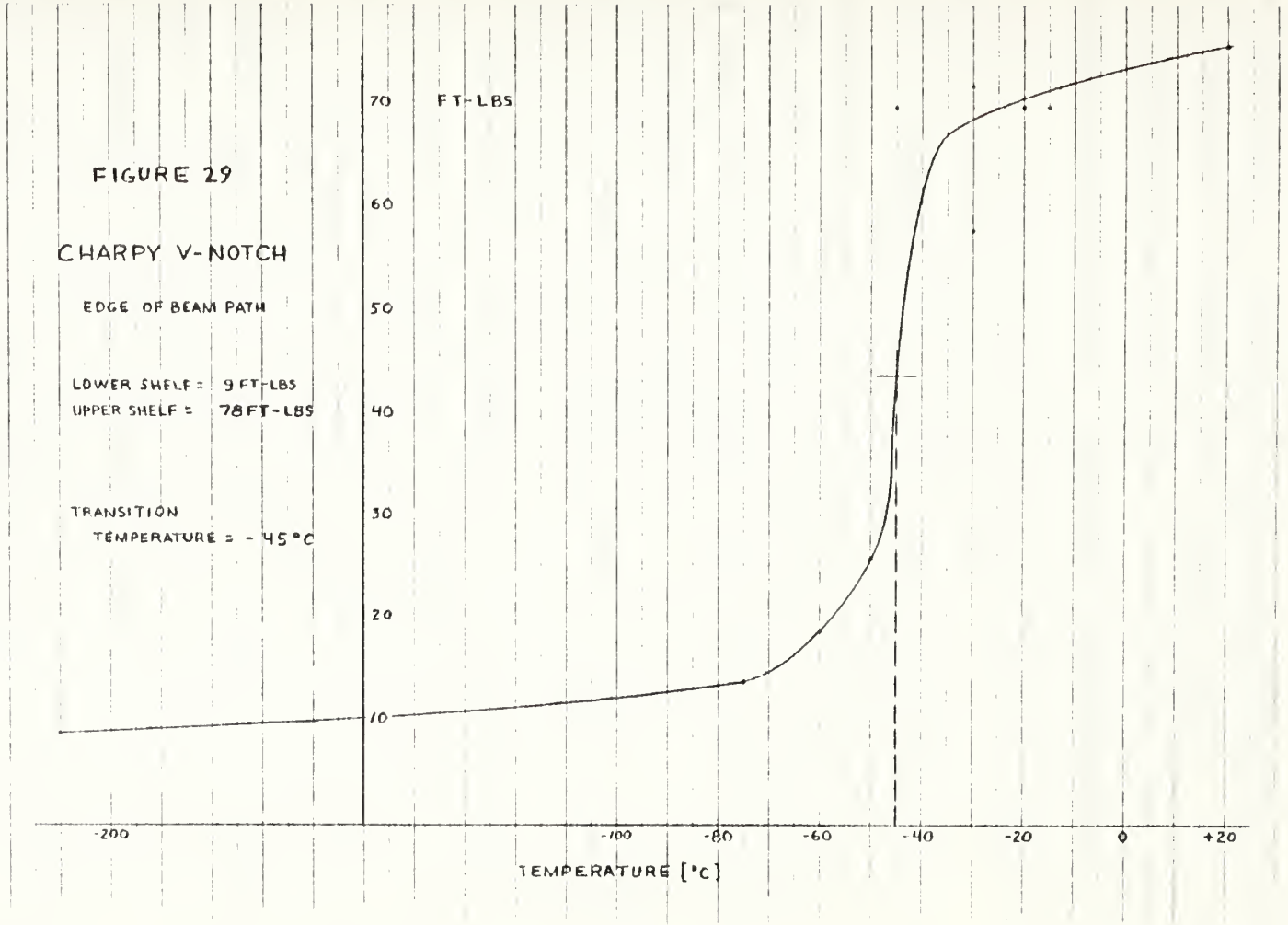
FIGURE 29
CHARPY V-NOTCH
EDGE OF BEAM PATH
LOWER SHELF = 9 FT-LBS
UPPER SHELF = 78 FT-LBS
TRANSITION TEMPERATURE = -45°C
70
60
50
40
30
20
10
FT-LBS
-200
-100
-80
-60
-40
-20
0
+20
TEMPERATURE [°C]

7. CHEMICAL ANALYSIS OF THE BENT PLATES

X-ray microprobe chemical analysis was attempted for the alloying elements in samples from Plates 1 and 2. It was hoped to be determined which metals were being segregated from the matrix as carbides. Manganese and molybdenum were found to be present in quantities too small to measure, although they did show up qualitatively.

A line analysis was performed, paralleling the row of diamond indentures from the hardness testing and taking a spot analysis at every second hardness point. The elements analyzed were nickel and chrome, with iron and silicon measured to confirm the accuracy.

Table 13 is a summary of the analysis of Plate 1. Table 14 is the analysis of Plate 2.

The line analyses are presented in Figures 30 and 31. There is a regular variation of the concentration of both metals in the underlying plate. This phenomenon was observed by the Welding Institute study[35] to correspond with the carbide banding of HY-80 plates. Figure 1 illustrates that there is a higher concentration of both nickel and chrome in carbides near the irradiated surface of Plate 1.

Figure 31 shows a higher concentration of nickel carbides in certain areas of the heat affected zones. Although the chromium carbide concentration varies over shorter distances, the magnitude of the concentration remains in a

range that is closer to the baseplate. The nickel line shows some regions, 0.5 to 0.7 mm thick, with little variation in concentration.

There is a general correspondence in each plate, between the nickel and chromium carbide concentration. There is no apparent correspondence between the chemical analyses and the hardness measurements.

The importance of the segregation of alloying elements from the metal matrix in the form of carbides lies in the great stability of the carbides. If the metal is tied up in a carbide crystal it does not contribute to those alloy properties for which it was added to the melt. In the case of nickel, it may cause degradation of the notch toughness of the alloy, as has been observed. In the case of chrome, it may increase the susceptibility of the surface to corrosion.

TABLE 13

CHEMICAL LINE ANALYSIS OF PLATE 1

Depth [mm]	Percent Nickel	Percent Chrome
0.08	3.53	2.21
0.25	3.16	2.06
0.45	3.14	1.89
0.65	3.02	1.97
0.85	2.96	1.90
1.06	3.06	1.88
1.26	3.13	1.94
1.47	3.03	1.94
1.67	3.00	1.90
1.88	3.02	1.93
2.09	3.12	2.01
2.30	3.04	1.94
2.50	2.91	1.94
2.71	3.02	1.90
3.12	3.13	1.93
3.32	2.97	1.88
3.55	3.05	1.97
Baseplate	3.17	1.93
Baseplate	3.16	1.97
Baseplate	2.99	1.90
Baseplate	3.25	2.06
Baseplate average	3.14	1.97

TABLE 14

CHEMICAL LINE ANALYSIS OF PLATE 2

Depth [mm]	Percent Nickel	Percent Chrome
0.10	2.96	1.87
0.42	2.90	1.92
0.63	3.19	1.88
0.83	3.17	1.95
1.03	3.08	1.98
1.23	2.97	1.93
1.53	3.25	2.07
1.73	3.09	1.93
1.93	3.01	1.95
2.13	3.01	1.89
2.33	3.05	2.02
2.55	3.02	1.92
2.76	3.35	2.01
2.96	3.11	2.00
3.16	3.08	1.98
3.38	2.89	1.88
3.59	3.02	1.91
3.79	3.14	1.95
3.89	3.25	1.95
4.11	3.31	2.03
4.33	2.96	1.95

TABLE 14 (CONTINUED)

Depth [mm]	Percent Nickel	Percent Chrome
4.55	2.95	1.91
4.78	2.95	1.96
4.99	3.11	2.02
5.21	3.11	1.97
5.44	3.12	1.96
5.68	2.91	1.89
5.90	2.93	1.95
6.13	2.95	1.87
6.37	2.93	1.82
7.14	3.26	1.95
7.78	3.15	1.87
8.39	3.20	2.01
9.25	3.00	1.84
9.88	3.06	1.94
10.53	2.99	1.96
11.17	3.08	1.89
11.79	2.99	1.96
12.40	3.00	1.92
13.01	3.12	1.92

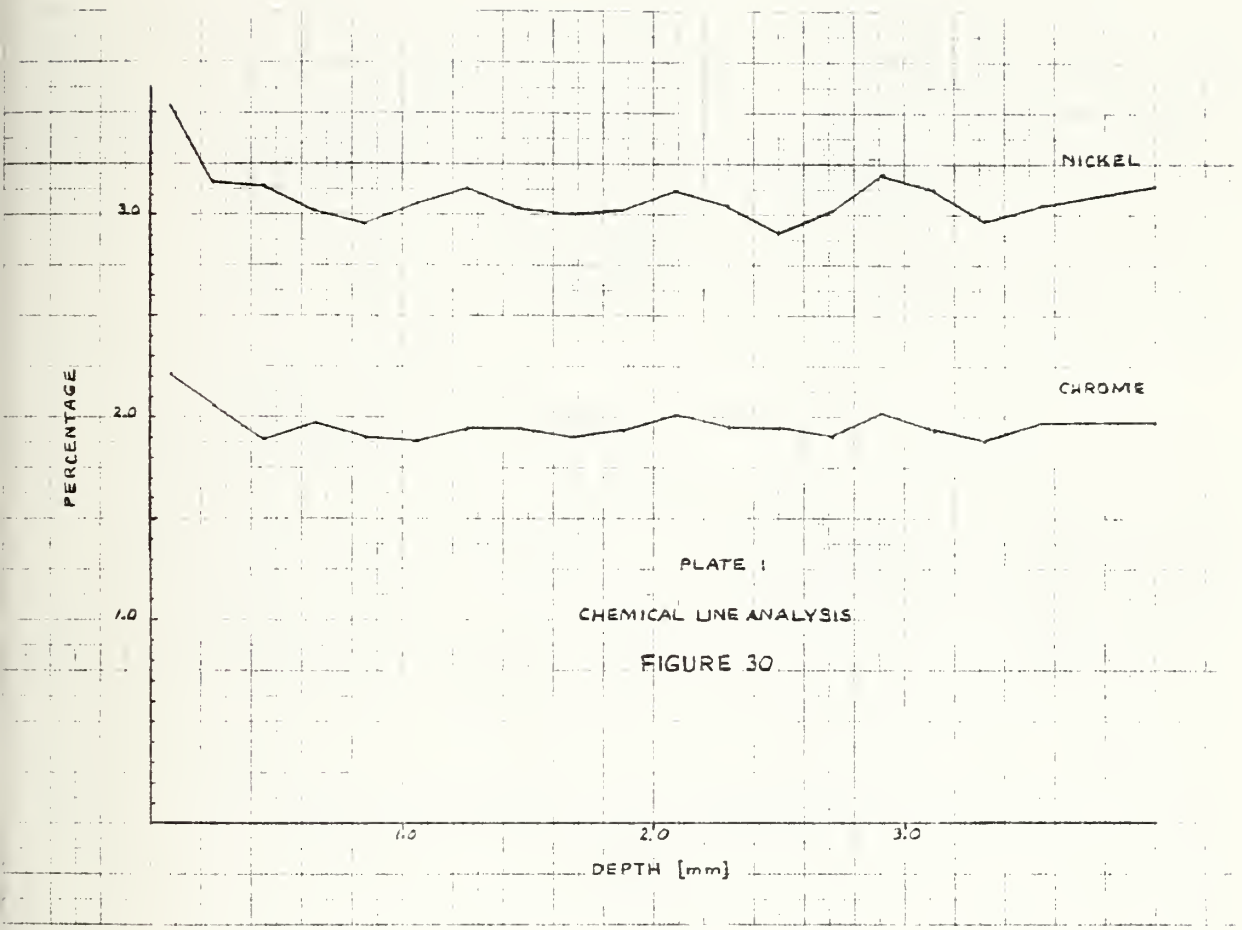

PLATE I

CHEMICAL LINE ANALYSIS

FIGURE 30

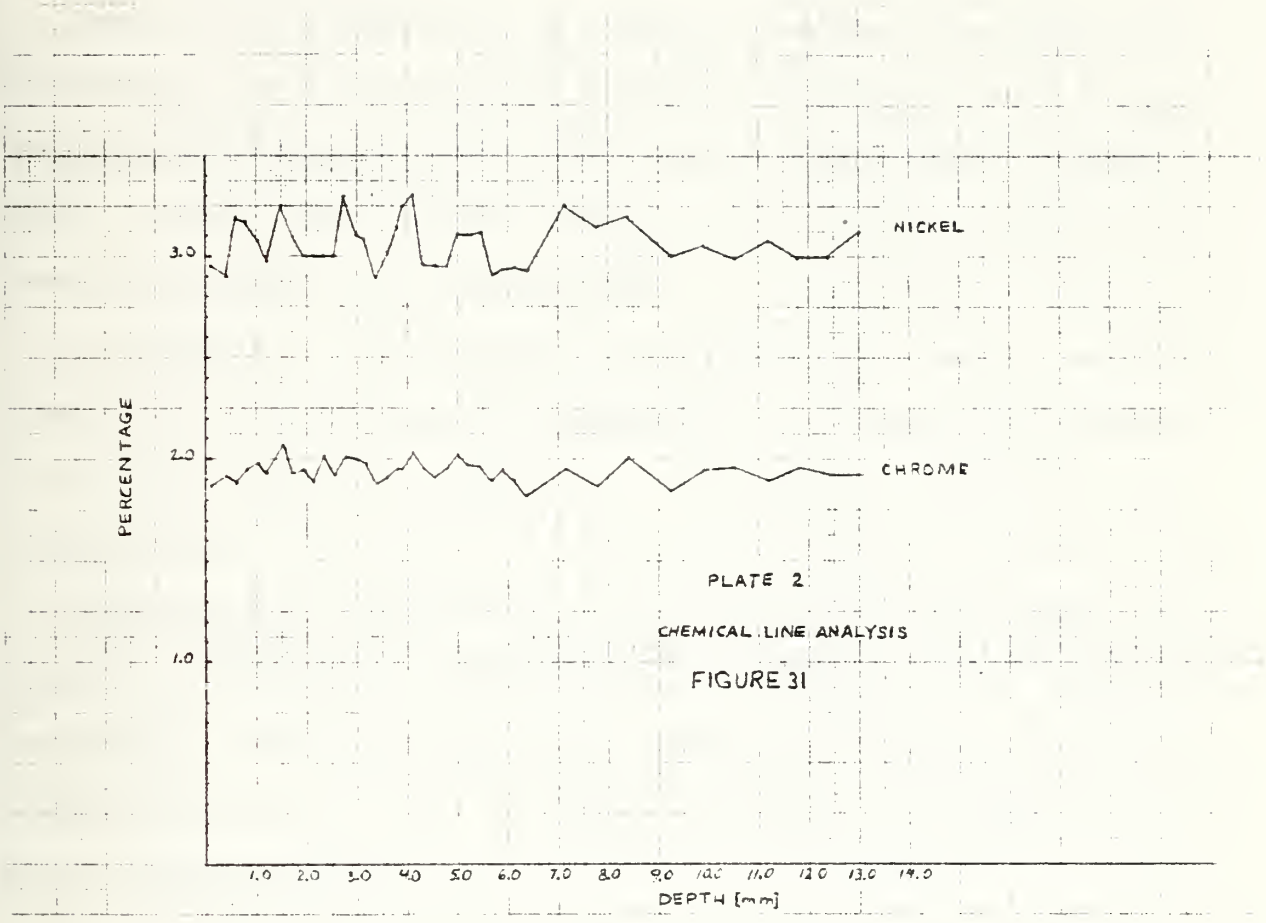

PLATE 2

CHEMICAL LINE ANALYSIS

FIGURE 31

8. CONCLUSIONS

Laser line heating is a feasible method for removing distortion or forming large plates, from the point-of-view of material degradation. The heat affected zone produced with a laser bend is very shallow and has small effect on the mass properties of the plate.

Although a single-pass procedure is more energy efficient, it produces considerably more material damage than a multiple-pass procedure. Therefore, the latter is recommended.

Metallographic examination revealed that the depth of damage is proportional to the angle of bend for a single-pass bend. For a multiple-pass bend, the maximum depth of damage is about 2.1 mm. It does not appear to increase with each additional pass.

The single-pass bends were characterized by excessive grain growth in Zone 1, while the multiple-pass case actually resulted in grain refinement. Based upon the microstructure of the heat affected zone, it is recommended that the process use a laser power of 7 kW and a travel speed of 12 in/min or any combination that results in the production of an equivalent surface temperature. Figure 32 is a graph of possible combinations of laser power and travel speed to produce surface temperatures the same as experienced by Plate 1 in this experiment.

Because of the temperature gradient within the metal, it is unlikely that a method can be devised to eliminate the carbide segregation in Zone 2. Rather, the zone should be kept as small as possible, again recommending the multiple-pass procedure.

The measured high hardness in the heat affected zone is due to a composition of untempered martensite. It may be possible to use an additional pass of the laser, after the plate has cooled from its original line-heating, to temper the surface. This will reduce the hardness and increase the strength of the surface layer at least.

The microhardness measurements confirm the recommendation of a multiple-pass procedure. The depth of the hardened zone appeared to reach a maximum of 2.0 mm after the second pass. The third pass increased the peak hardness value, but did not extend the hardened zone deeper into the plate.

The microcracks that were observed while measuring the surface hardness of Plate 2 are believed to be confined to the surface layer of grains and to have been caused by the apparent near liquation of this layer. It is not expected to be a problem in bends made with lower surface temperatures.

The most serious degradation was in notch toughness. The loss of toughness both at the center and the edge of the heat affected zone could make the process unacceptable for

use in naval structures. Surface tempering subsequent to line bending may restore some of the lost toughness.

The apparent loss of nickel from the matrix in the damaged zone implies that it will not be possible to completely restore the notch toughness. The loss of chrome, on the other hand, introduces the possibility of corrosion problems at the burn.

Based on the results of this study, additional research is indicated. It is recommended that an additional set of at least twelve plates be bent. All the test plates should be from the same heat of steel, and if possible from the same rolled plate and with the same orientation to the rolling direction. These plates should be instrumented with thermocouples and strain gauges on the top and the bottom. They should be divided into two groups. One group to be bent in a single pass of the laser at 7 kW and a travel speed of 6 in/min. The other group should be bent with 4 passes of the laser at 7 kW and a travel speed of 12 in/min. This should give approximately equal angles of bend.

On three plates from each group, a temper pass should be made after complete cooling. The proper surface temperature can be obtained with a travel speed of 70 in/min at a power level of 7kW or with a combination from the temper curve on Figure 32. These figures are calculated with the formula for surface temperature by Ready which is given is Chapter 2.

This will yield 4 sets of plates, the members of each set having been identically processed. Of each set, one plate should be cut up for metallographic examination, microhardness measurement and x-ray microprobe analysis. A second plate should be made into full-scale Charpy bars. These bars should be broken on a standard Charpy machine with better temperature equilibration than in the initial series of tests. The third plate in each set should be cut into standard tension test samples across the burn. The engineering stress-strain curve for these samples should be obtained and compared with samples from the same heat, rolled plate and orientation to the rolling direction.

Calorimetric samples of HY-80 and any other metals of interest should be prepared so that the absorbance of each at the frequency of the laser can be determined. This quantity is required to accurately calculate the heat input.

An additional experiment should be run to test the efficacy of immediate water quenching of the burn surface while irradiating. Care will need to be taken that the water does not flow onto the irradiated spot. Water absorbs infrared light and will therefore block the beam. The entire plate acted as a heat sink in the current series of experiments. The surface formation of martensite indicates that the quench rate by conduction is already quite high. This suggests that a water quench on the surface may make no

difference in the final structure. However, it would be worthwhile to try it.

A third experiment should be conducted to compare the corrosion behavior of a laser bent plate and an unbent plate. It would be worthwhile to try a number of environments, but splash zone and marine atmosphere tests are essential in light of the loss of chrome from the metal near the surface.

A set of fatigue tests would be informative, particularly low cycle fatigue which is a concern for ship hulls.

A similar series of experiments should be run for other metals of interest for ship hulls, particularly high strength low-alloy steels and titanium alloy. The lower carbon content of HSLA steel may lead to less carbide segregation than occurs with HY-80. Titanium alloy may have oxidation problems at the burn due to the high temperature and may therefore require a shielding gas. In any case, it is essential that the precise absorbance of each material of interest be determined so that accurate formulas can be devised to describe the heat input and bending process.

Finally, a series of experiments should be conducted in an attempt to produce different shapes. The advantages of a laser over a brake press are the directability and controlability of the beam. By placing bend lines close together, it may be possible to produce a continuous curve.

By crossing bend lines, it may be possible to produce complex and compound curves like those required for a submarine hull or the flare of a ship bow. By producing a circular pattern, it may be possible to dish a plate.

The superior controllability of the process should make it possible to devise a fully automatic computer-operated system for forming plates. Ideally, a CADCAM program could be written that would except the desired plate shape as an input and would calculate the necessary laser parameters and heating pattern, load the plate to the worksite, irradiate the plate and produce the requested formed plate as an output. Current processes of plate forming are all very labor intensive. The laser line bending method can be used for more shapes than brake press forming and is more controllabe than explosive forming. The degree of material damage is small if a multiple-pass procedure is used, and might be even smaller with a tempering pass. The method is feasible, and deserving of further study.

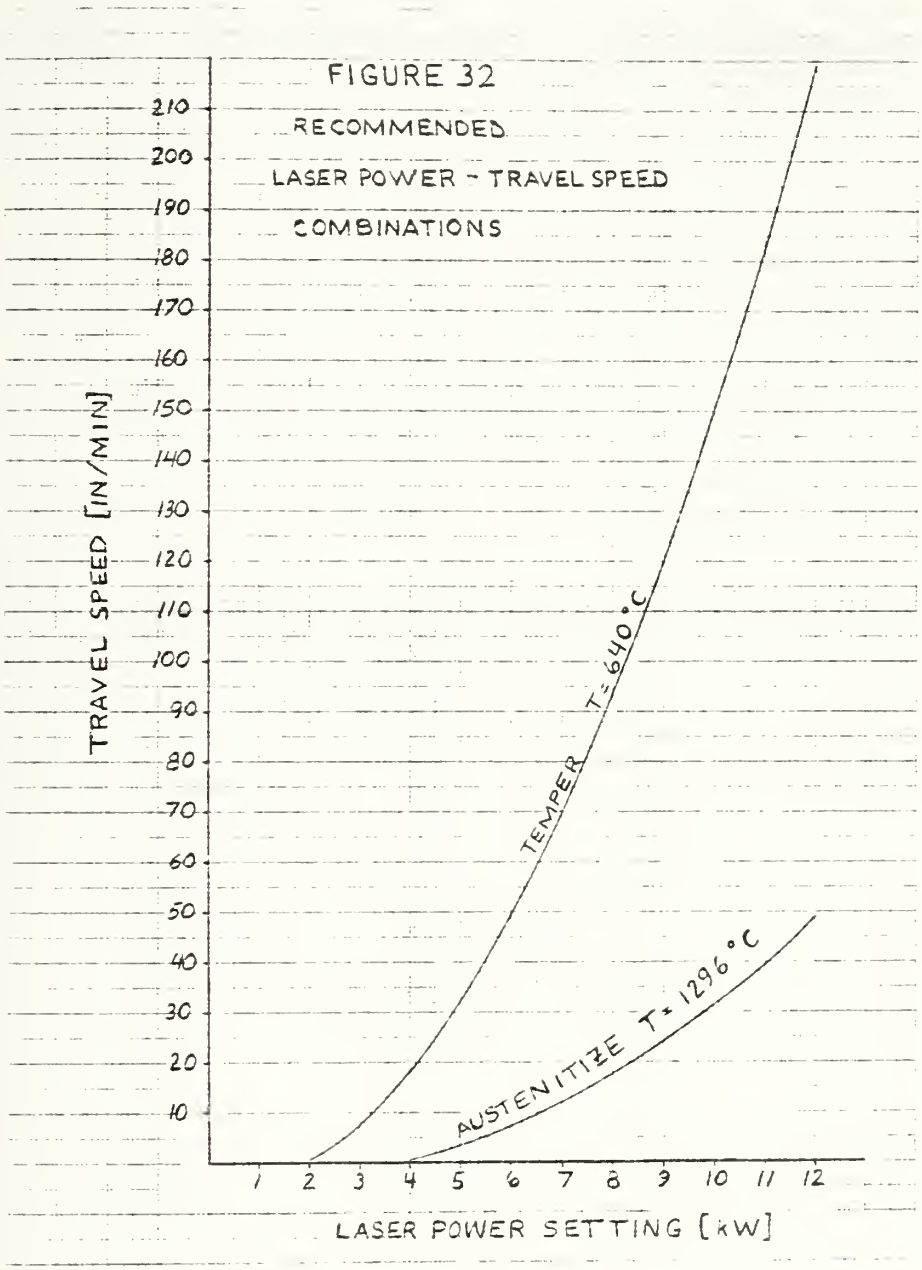
FIGURE 32
RECOMMENDED
LASER POWER - TRAVEL SPEED
COMBINATIONS
TRAVEL SPEED [IN/MIN]
210
200
190
180
170
160
150
140
130
120
110
100
90
80
70
60
50
40
30
20
10
TEMPER T=640°C
AUSTENITIZE T=1296°C
1 2 3 4 5 6 7 8 9 10 11 12
LASER POWER SETTING [kW]

FIGURE 32

RECOMMENDED LASER POWER - TRAVEL SPEED COMBINATIONS

REFERENCES

1. Koichi Masubuchi; Proposal on Laser Forming of Steel Plates for Ship Construction; submitted to the Naval Material Command, Department of the Navy, Washington, D.C.; November, 1982; p. 5.

2. J. F. Ready; "The Influence of the Laser-Surface Interaction on Industrial Application"; Lasers in Modern Industry; p. 73.

3. J. F. Ready; Industrial Applications of High Power Laser Technology; Proceedingd of the Society of Photo-optical Instrumentation Engineers, San Diego, CA, 24-25 August 1976; p. 139.

4. Simon Engel; "Basics of Laser Heat Treating"; Lasers in Modern Industry; p. 108.

5. J. F. Ready; "Effects of Laser Radiation on Solids"; Laser Welding and Machining; p. 87-92.

6. E. M. Breinan, B. H. Kear, L. E. Greenwald and C. M. Banas; "Laser Glazing - A New Process for Production and Control of Rapidly-Chilled Metallurgical Microstructures"; Lasers in Modern Industry.

7. John F. Ready; Effects of High-Power Laser Radiation; Academic Press, NY, 1971; p. 82.

8. Technical Report of Research on Metal Working by High Power Laser; High Power Laser Committee of the Japan Welding Society, 26 September 1983; p. 364. (In Japanese)

9. The Metallurgy and Welding of QT35 and HY-80 Steels; The Welding Institute, Abington, Cambridge, England, 1974; p. 3.

10. Preceeding citation, p. 9.

11. Military Specification, MIL-S-16216J, Steel Plate, Alloy, Structural, High Yield Strength (HY-80 and HY-100), 15 March 1972; p. 3-4.

12. William F. Smith; Structures and Properties of Engineering Alloys; McGraw-Hill, NY, 1981; p. 117-151.

REFERENCES (CONTINUED)

13. The Making, Shaping and Treating of Steel, 9th Ed.; United Stated Steel Corp., 1971; p. 1081-1082.

14. MIL-S-16216J; p. 4.

15. U. S. Steel Corp.; p. 590-595.

16. U. S. Steel Corp.; p. 727.

17. U. S. Steel Corp.; p. 1075-1078.

18. Metallography, Structures and Phase Diagrams; Metals Handbook, Volume 8; American Society for Metals, 1973; p. 276.

19. William F. Smith; p. 25-43.

20. U. S. Steel Corp.; p. 1089.

21. U. S. Steel Corp.; p. 1096.

22. R. W. Flax, R. E. Keith and M. D. Randall; Welding the HY-80 Steels, ASTM Special Technical Publication 494; American Society for Teating and Materials, 1971; p. 8.

23. U. S. Steel Corp.; p. 1091-1102.

24. U. S. Steel Corp.; p. 1092.

25. Welding Institute; p. 10-11.

26. MIL-S-16216J; p. 5.

27. MIL-S-16216J; p. 22.

28. Welding Institute; p. 11-13.

29. Welding Institute; p. 18.

30. R. W. Flax et al.; p. 11.

31. Welding Institute; p. 23.

32. Welding Institute; p. 8-9.

33. H. C. Child; Surface Hardening of Steel; Design Council, Oxford University Press, 1980; Engineering Design Guides No. 37; p. 1-4.

34. Properties and Selection; Metals Handbook, Volume 1; American Society for Metals, 1961; p. 189.

35. Welding Institute; p. 16.

207060

Thesis
D18247 Deacon
Material degradation in heavy steel plates caused by bending with a laser.

3 MAR 83 14514

207060

Thesis
D18247 Deacon
Material degradation in heavy steel plates caused by bending with a laser.

thesD18247
Material degradation in heavy steel plat
3 2768 002 10069 5
DUDLEY KNOX LIBRARY